Ill posedness in modelling two-dimensional morphodynamic problems
Effects of bed slope and secondary flow

Chavarrías, Víctor; Schielen, Ralph; Ottevanger, Willem; Blom, Astrid

Important note
To cite this publication, please use the final published version (if applicable).
Please check the document version above.

Ill-posedness in modelling 2D morphodynamic problems: Effects of bed slope and secondary flow

Víctor Chavarrías [*1], Ralph Schielen[2,3], Willem Ottevanger[4], and Astrid Blom[1]

[1]Faculty of Civil Engineering and Geosciences, Delft University of Technology, Delft, The Netherlands.

[2]Faculty of Engineering Technology, University of Twente, Enschede, The Netherlands.

[3]Ministry of Infrastructure and Water Management-DG Rijkswaterstaat, Lelystad, The Netherlands.

[4]Deltares, Delft, The Netherlands.

14$^{\text{th}}$ February, 2019

Abstract

A two-dimensional model describing river morphodynamic processes under mixed-size sediment conditions is analysed with respect to its well-posedness. Well-posedness guarantees the existence of a unique solution continuously depending on the problem data. When a model becomes ill-posed, infinitesimal perturbations to a solution grow infinitely fast. Apart from the fact that this behaviour cannot represent a physical process, numerical simulations of an ill-posed model continue to change as the grid is refined. For this reason, ill-posed models cannot be used as predictive tools. One source of ill-posedness is due to the simplified description of the processes related to vertical mixing of sediment. The current analysis reveals the existence of two additional mechanisms that lead to model ill-posedness: secondary flow due to the flow curvature and the gravitational pull on the sediment transport direction. When parametrising secondary flow, accounting for diffusion in the transport of secondary flow intensity is a requirement for obtaining a well-posed model. When considering the theoretical amount of diffusion, the model predicts instability of perturbations that are incompatible with the shallow water assumption. The gravitational pull is a necessary mechanism to yield a well-posed model, but not all closure relations to account for this mechanism are valid under mixed-size sediment conditions. Numerical simulations of idealised situations confirm the results of the stability analysis and highlight the consequences of ill-posedness.

---

*Corresponding author: `v.chavarriasborras@tudelft.nl`

1 Introduction

Modelling of fluvial morphodynamic processes is a powerful tool not only to predict the future state of a river after, for instance, an intervention or a change in the discharge regime (*Blom et al.*, 2017), but also as a source of understanding of the natural processes responsible for patterns such as dunes, meanders, and bars (*Callander*, 1969; *Seminara*, 2006; *Colombini and Stocchino*, 2012). A framework for modelling the morphodynamic development of alluvial rivers is composed of a system of partial differential equations for modelling the flow, change in bed elevation, and change in the bed surface texture. The *Saint-Venant* (1871) equations account for conservation of water mass and momentum and enable modelling processes with a characteristic length scale significantly longer than the flow depth in one-dimensional cases. The Shallow Water Equations describe the depth-averaged flow in two-dimensional cases. Conservation of unisize bed sediment is typically modelled using the *Exner* (1920) equation and, under mixed-size sediment conditions, the active layer model (*Hirano*, 1971) accounts for mass conservation of bed sediment of each grain size.

Although widely successful in predicting river morphodynamics, a fundamental problem arises when using the above framework. Under certain conditions the description of the natural phenomena is not captured by the system of equations, which manifests as an ill-posed model. Models describe a simplified version of reality, which allows us to understand the key elements playing a major role in the dynamics of the system one studies (*Paola and Leeder*, 2011). Major simplifications such as reducing streamwise morphodynamic processes to a diffusion equation allow for insight on the creation of stratigraphic records and evolution on large spatial scales (*Paola et al.*, 1992; *Paola*, 2000; *Paola and Leeder*, 2011). There is a difference between greatly simplified models and models that do not capture the physical processes. A simplified model reproduces a reduced-complexity version of reality (*Murray*, 2007) and it is mathematically well-posed, as a unique solution exists that depends continuously on the data (*Hadamard*, 1923; *Joseph and Saut*, 1990). An ill-posed model lacks crucial physical processes that cause the model to be unsuitable to capture the dynamics of the system (*Fowler*, 1997). An ill-posed model is unrepresentative of a physical phenomenon, as the growth rate of infinitesimal perturbations to a solution (i.e., negligible noise from a physical perspective) tends to infinity (*Kabanikhin*, 2008). This is different from chaotic systems, in which noise similarly causes the solution to diverge but not infinitely fast (*Devaney*, 1989; *Banks et al.*, 1992).

An example of an ill-posed model is the one describing the dynamics of granular flow. The continuum formulation of such a problem depends on deriving a model for the granular viscosity. *Jop et al.* (2005, 2006) relate viscosity to a dimensionless shear rate. The model captures the dynamics of granular flows if the dimensionless shear rate is within a certain range, but otherwise the model is ill-posed and loses its predictive capabilities (*Barker et al.*, 2015). A better representation of the physical processes guaranteeing that viscosity tends to 0 when the dimensionless shear rate tends

⁶³ to 0 extends the domain of well-posedness (*Barker and Gray*, 2017).

⁶⁴   Under unisize sediment and one-dimensional flow conditions, the Saint-Venant-Exner model

⁶⁵ may be ill-posed when the Froude number is larger than 6 (*Cordier et al.*, 2011). As most flows

⁶⁶ of interest are well below this limit, we can consider modelling of fluvial problems under unisize

⁶⁷ sediment conditions to be well-posed. This is not the case when considering mixed-size sediment.

⁶⁸ Using the active layer model we assume that the bed can be discretised into two layers: the active

⁶⁹ layer and the substrate. The sediment transport rate depends on the grain size distribution of

⁷⁰ the active layer. A vertical flux of sediment occurs between the active layer and the substrate if

⁷¹ the elevation of the interface between the active layer and the substrate changes. The active layer

⁷² is well-mixed, whereas the substrate can be stratified. The above simplification of the physical

⁷³ processes responsible for vertical mixing causes the active layer model to be ill-posed (*Ribberink*,

⁷⁴ 1987; *Stecca et al.*, 2014; *Chavarrías et al.*, 2018). In particular, the active layer is prone to be ill-

⁷⁵ posed under degradational conditions into a substrate finer than the active layer (i.e., an armoured

⁷⁶ bed (*Parker and Sutherland*, 1990)) for any value of the Froude number.

⁷⁷   Previous analyses of river morphodynamic models regarding their well-posedness have been

⁷⁸ focused on conditions of one-dimensional flow (*Ribberink*, 1987; *Cordier et al.*, 2011; *Stecca et al.*,

⁷⁹ 2014; *Chavarrías et al.*, 2018). Our objective is to extend these analyses to conditions of two-

⁸⁰ dimensional flow. More specifically we include the secondary flow and the bed slope effect in the

⁸¹ analysis of the well-posedness of the system of equations.

⁸²   As the flow is intrinsically three-dimensional, the depth-averaging procedure eliminates an

⁸³ important flow component: the secondary flow (*Van Bendegom*, 1947; *Rozovskii*, 1957). The

⁸⁴ secondary flow causes, for instance, an increase in the amplitude of meanders (*Kitanidis and*

⁸⁵ *Kennedy*, 1984) and plays an important role in bar development (*Olesen*, 1982). To understand the

⁸⁶ morphology of two-dimensional features, it is necessary to account for the fact that the sediment

⁸⁷ transport direction is affected by the gravitational pull when the bed slope in the transverse

⁸⁸ direction is significant (*Dietrich and Smith*, 1984; *Seminara*, 2006). This is usually done using

⁸⁹ a closure relation that sets the angle between the flow and the sediment transport directions as

⁹⁰ a function of the flow and sediment parameters (*Van Bendegom*, 1947; *Engelund*, 1974; *Talmon*

⁹¹ *et al.*, 1995; *Seminara et al.*, 2002; *Parker et al.*, 2003; *Francalanci and Solari*, 2007, 2008; *Baar*

⁹² *et al.*, 2018).

⁹³   In this paper we show that combining these two effects, secondary flow and sediment deflection

⁹⁴ by the bed slope, leads in some cases to an ill-posed system of equations. The paper is organised

⁹⁵ as follows. In Section 2 we present the model equations describing the primary and secondary flow,

⁹⁶ as well as changes in bed elevation and surface texture. In Section 3 we extend the explanation of

⁹⁷ ill-posedness and relate it to growth of perturbations. We subsequently conduct a stability analysis

⁹⁸ of the equations, which indicates the conditions under which the secondary flow model and the

⁹⁹ closure relation for the bed slope effect yield an ill-posed model (Section 4). In Section 5 we run

100 numerical simulations of idealised cases to test the validity of the analytical results and study the

101 consequences of ill-posedness.

2   Mathematical Model

103 In this section we present the two-dimensional mathematical model of flow, accounting for sec-

104 ondary flow, coupled to a morphodynamic model for mixed-size sediment. We subsequently intro-

105 duce the equations describing the primary flow (Section 2.1), the secondary flow (Section 2.2), and

106 morphodynamic change (Section 2.3). In Section 2.4 we linearise the system of equations to study

107 the stability of perturbations.

2.1   Primary Flow Equations

109 The primary flow is described using the depth-averaged Shallow Water Equations (e.g. *Vreugdenhil*,

110 1994):

$$\frac{\partial h}{\partial t} + \frac{\partial q_{\mathrm{x}}}{\partial x} + \frac{\partial q_{\mathrm{y}}}{\partial y} = 0 \,, \tag{1}$$

$$\frac{\partial q_{\mathrm{x}}}{\partial t} + \frac{\partial (q_{\mathrm{x}}^2/h + gh^2/2)}{\partial x} + \frac{\partial \left(\frac{q_{\mathrm{x}} q_{\mathrm{y}}}{h} \right)}{\partial y} + gh\frac{\partial \eta}{\partial x} - F_{\mathrm{sx}} =$$
$$= 2\frac{\partial}{\partial x} \left(\nu h \frac{\partial (\frac{q_{\mathrm{x}}}{h})}{\partial x} \right) + \frac{\partial}{\partial y} \left(\nu h \left(\frac{\partial (\frac{q_{\mathrm{x}}}{h})}{\partial y} + \frac{\partial (\frac{q_{\mathrm{y}}}{h})}{\partial x} \right) \right) - ghS_{\mathrm{fx}} \,, \tag{2}$$

$$\frac{\partial q_{\mathrm{y}}}{\partial t} + \frac{\partial (q_{\mathrm{y}}^2/h + gh^2/2)}{\partial y} + \frac{\partial \left(\frac{q_{\mathrm{x}} q_{\mathrm{y}}}{h} \right)}{\partial x} + gh\frac{\partial \eta}{\partial y} - F_{\mathrm{sy}} =$$
$$2\frac{\partial}{\partial y} \left(\nu h \frac{\partial (\frac{q_{\mathrm{y}}}{h})}{\partial y} \right) + \frac{\partial}{\partial x} \left(\nu h \left(\frac{\partial (\frac{q_{\mathrm{y}}}{h})}{\partial x} + \frac{\partial (\frac{q_{\mathrm{x}}}{h})}{\partial y} \right) \right) - ghS_{\mathrm{fy}} \,, \tag{3}$$

116 where (x, y) [m] are Cartesian coordinates and t [s] is the time coordinate. The variables $(q_{\mathrm{x}}, q_{\mathrm{y}}) =$

117 (uh, vh) [m²/s] are the specific water discharges in the x and y direction, respectively, where h

118 [m] is the flow depth and u [m/s] and v [m/s] are the depth-averaged flow velocities. The variable

119 η [m] is the bed elevation and g [m/s²] the acceleration due to gravity. The friction slopes are

120 $(S_{\mathrm{fx}}, S_{\mathrm{fy}})$ [−] and the diffusion coefficient ν [m²/s] is the horizontal eddy viscosity. The depth-

121 averaging procedure of the equations of motion introduces terms that originate from the difference

122 between the actual velocity at a certain elevation in the water column and the depth-averaged

123 velocity. We separate the contributions due to turbulent motion and secondary flow caused by

124 the flow curvature. The contribution due to turbulent motion is accounted for by the diffusion

125 coefficient. *Elder* (1959) derived an expression for the diffusion coefficient that accounts for the

126 effect of turbulent motion on the depth-averaged flow assuming a logarithmic profile for the primary

127 flow and negligible effect of molecular viscosity:

$$\nu_{\mathrm{E}} = \frac{1}{6}\kappa h u^* \,, \tag{4}$$

129   where $\kappa = 0.41$ [−] is the Von Kármán constant and $u^* = \sqrt{C_\mathrm{f}}Q/h$ [m/s] is the friction velocity.

130   Parameter C_f [−] is a nondimensional friction coefficient, which we assume to be constant (*Ikeda*

131   *et al.*, 1981; *Schielen et al.*, 1993) and $Q = \sqrt{q_\mathrm{x}^2 + q_\mathrm{y}^2}$ [m²/s] is the module of the specific water

132   discharge. In the numerical simulations we will assume the eddy viscosity to be a constant equal

133   to the value given by ν_E in a reference state (e.g. *Falconer*, 1980; *Lien et al.*, 1999). Appendix A

134   presents the limitations of the coefficient derived by *Elder* (1959).

135   The terms $(F_\mathrm{sx}, F_\mathrm{sy})$ [m²/s²] account for the effect of secondary flow. These terms are respon-

136   sible for a transfer of momentum that shifts the maximum velocity to the outer bend (*Kalkwijk*

137   *and De Vriend*, 1980), as well as for a sink of energy in the secondary circulation (*Flokstra*, 1977;

138   *Begnudelli et al.*, 2010). We deal with these terms in Section 2.2.

139   We assume a Chézy-type friction:

$$S_\mathrm{fx} = \frac{C_\mathrm{f}q_\mathrm{x}Q}{gh^3} \; , \quad S_\mathrm{fy} = \frac{C_\mathrm{f}q_\mathrm{y}Q}{gh^3} \; . \tag{5}$$

141   One underlying assumption of the system of equations presented above is that the vertical length

142   and velocity scales are negligible with respect to the horizontal ones. Another assumption is the

143   fact that the concentration of sediment (the ratio between the solid and liquid discharge) is small

144   (below 6×10^{-3} (*Garegnani et al.*, 2011, 2013)), such that we apply the clear water approximation.

2.2 Secondary Flow Equations

146   This section describes the equations that model secondary flow (i.e., formulations for F_sx and F_sy

147   in equations (2) and (3)). The secondary flow velocity profile u^s [m/s] (i.e., the vertical profile

148   of the velocity component perpendicular to the primary flow) is assumed to have a universal

149   shape as a function of the relative elevation in the water column $\zeta = (z - \eta)/h$ [−], where z

150   [m] is the vertical Cartesian coordinate perpendicular to x and y increasing in upward direction

151   (*Rozovskii*, 1957; *Engelund*, 1974; *De Vriend*, 1977, 1981; *Booij and Pennekamp*, 1984). Worded

152   differently, the vertical profile of the secondary flow is parametrised by a single value representing

153   the intensity of the secondary flow I [m/s], such that $u^\mathrm{s} = f(\zeta)I$. The secondary flow intensity I is

154   the integral of the absolute value of the secondary flow velocity profile (*De Vriend*, 1981). Among

155   others, *Rozovskii* (1957), *Engelund* (1974), and *De Vriend* (1977), derive equilibrium profiles of

156   the secondary flow that differ in the description of the eddy viscosity, vertical profile of the primary

157   flow, and the boundary condition of the flow at the bed. Following *De Vriend* (1977), we assume

158   a logarithmic profile for the primary flow (i.e., a parabolic distribution of the eddy viscosity) and

159   vanishing velocity close to the bed at $\zeta = \exp{(-1 - 1/\alpha)}$ where $\alpha = \frac{\sqrt{C_\mathrm{f}}}{\kappa} < 0.5$.

160   The depth-averaging procedure yields the integral value (along z) of the force per unit mass

161   that the secondary flow exerts on the primary flow (*De Vriend*, 1977; *Kalkwijk and De Vriend*,

1980):

$$F_{\text{sx}} = \frac{\partial T_{\text{xx}}}{\partial x} + \frac{\partial T_{xy}}{\partial y} \ , \tag{6}$$

$$F_{\text{sy}} = \frac{\partial T_{\text{yx}}}{\partial x} + \frac{\partial T_{\text{yy}}}{\partial y} \ , \tag{7}$$

where T_{lm} [m^3/s^2] is the integral shear stress per unit mass in the direction l-m. Assuming a large width-to-depth ratio (i.e., $B/h \gg 1$, where B [m] is the characteristic channel width) and a mild curvature (i.e., $h/R_\text{s} \ll 1$, where R_s [m] is the radius of curvature of the streamlines), the shear stress terms are:

$$T_{\text{xx}} = -2\frac{\beta^* I}{Q} q_\text{x} q_\text{y} \ , \tag{8}$$

$$T_{\text{xy}} = T_{\text{yx}} = \frac{\beta^* I}{Q} \left(q_\text{x}^2 - q_\text{y}^2 \right) \ , \tag{9}$$

$$T_{\text{yy}} = T_{\text{yy}} = 2\frac{\beta^* I}{Q} q_\text{x} q_\text{y} \ , \tag{10}$$

where $\beta^* = 5\alpha - 15.6\alpha^2 + 37.5\alpha^3$.

The simplest strategy to account for secondary flow assumes that the secondary flow is fully developed. This is equivalent to saying that the secondary flow intensity is equal to the equilibrium value $I_\text{e} = Q/R_\text{s}$ [m/s] found in an infinitely long bend (*Rozovskii*, 1957; *Engelund*, 1974; *De Vriend*, 1977, 1981; *Booij and Pennekamp*, 1983). A change in channel curvature leads to the streamwise adaptation of secondary flow to the equilibrium value (*De Vriend*, 1981; *Ikeda and Nishimura*, 1986; *Johannesson and Parker*, 1989; *Seminara and Tubino*, 1989). *Booij and Pennekamp* (1984) and *Kalkwijk and Booij* (1986) not only account for the spatial adaptation but also the temporal adaptation of the secondary flow associated with a variable discharge or tides. Here we adopt the latter strategy, which has been applied, for instance, in modelling the morphodynamics of braided rivers (*Javernick et al.*, 2016; *Williams et al.*, 2016; *Javernick et al.*, 2018). The spatial and temporal adaptation of secondary flow is expressed by (*Jagers*, 2003):

$$\frac{\partial I}{\partial t} + \frac{q_\text{x}}{h}\frac{\partial I}{\partial x} + \frac{q_\text{y}}{h}\frac{\partial I}{\partial y} - \frac{\partial}{\partial x}\left(\nu\frac{\partial I}{\partial x}\right) - \frac{\partial}{\partial y}\left(\nu\frac{\partial I}{\partial y}\right) = S_\text{s} \ , \tag{11}$$

where S_s [m/s^2] is a source term which depends on the difference between the local secondary flow intensity and its equilibrium value:

$$S_\text{s} = -\frac{I - I_\text{e}}{T_\text{I}} \ , \tag{12}$$

where T_I [s] is the adaptation time scale of the secondary flow:

$$T_\text{I} = \frac{L_\text{I} h}{Q} \ , \tag{13}$$

where $L_\text{I} = L_\text{I}^* h$ [m] is the adaptation length scale of the secondary flow, which depends on the nondimensional length scale $L_\text{I}^* = \frac{1-2\alpha}{2\kappa^2\alpha}$ (*Kalkwijk and Booij*, 1986).

195   The radius of curvature of the streamlines is defined as (e.g. *Legleiter and Kyriakidis*, 2006):

$$\frac{1}{R_\mathrm{s}} = \frac{\frac{\mathrm{d}x}{\mathrm{d}t}\frac{\mathrm{d}^2y}{\mathrm{d}t^2} - \frac{\mathrm{d}y}{\mathrm{d}t}\frac{\mathrm{d}^2x}{\mathrm{d}t^2}}{\left(\left(\frac{\mathrm{d}x}{\mathrm{d}t}\right)^2 + \left(\frac{\mathrm{d}y}{\mathrm{d}t}\right)^2\right)^{3/2}} \ , \tag{14}$$

197   assuming steady flow and in terms of water discharge we obtain:

$$\frac{1}{R_\mathrm{s}} = \frac{-q_\mathrm{x}q_\mathrm{y}\frac{\partial q_\mathrm{x}}{\partial x} + q_\mathrm{x}^2\frac{\partial q_\mathrm{y}}{\partial x} - q_\mathrm{y}^2\frac{\partial q_\mathrm{x}}{\partial y} + q_\mathrm{x}q_\mathrm{y}\frac{\partial q_\mathrm{y}}{\partial y}}{\left(q_\mathrm{x}^2 + q_\mathrm{y}^2\right)^{3/2}} \ . \tag{15}$$

199   The secondary flow model described in this section closes the primary flow model described in

200   Section 2.1 given a certain bed elevation. In the following section we describe the model equations

201   that describe changes in bed elevation as a function of the primary and secondary flow.

202   2.3   Morphodynamic Equations

203   We consider an alluvial bed composed of an arbitrary number N of non-cohesive sediment fractions

204   characterised by a grain size d_k [m], where the subscript k denotes the grain size fraction in

205   increasing order (i.e., $d_1 < d_2 < ... < d_N$). Bed elevation change depends on the divergence of the

206   sediment transport rate (*Exner*, 1920):

$$\frac{\partial \eta}{\partial t} + \frac{\partial q_\mathrm{bx}}{\partial x} + \frac{\partial q_\mathrm{by}}{\partial y} = 0 \ , \tag{16}$$

208   where $q_\mathrm{bx} = \sum_{k=1}^{N} q_{\mathrm{bx}k}$ [m²/s] and $q_\mathrm{by} = \sum_{k=1}^{N} q_{\mathrm{by}k}$ [m²/s] are the total specific (i.e., per unit of

209   differential length) sediment transport rates including pores in the x and y direction, respectively.

210   The variables $q_{\mathrm{bx}k}$ [m²/s] and $q_{\mathrm{by}k}$ [m²/s] are the specific sediment transport rates of size fraction

211   k including pores. For simplicity we assume a constant porosity and density of the bed sediment.

212   The sediment transport rate is assumed to be locally at capacity, which implies that we do not

213   model the temporal and spatial adaptation of the sediment transport rate to capacity conditions

214   (*Bell and Sutherland*, 1983; *Phillips and Sutherland*, 1989; *Jain*, 1992).

215   Changes in the bed surface grain size distribution are accounted for using the active layer model

216   (*Hirano*, 1971). For simplicity, we assume a constant active layer thickness L_a [m]. Conservation

217   of sediment mass of size fraction k in the active layer reads:

$$\frac{\partial M_{\mathrm{a}k}}{\partial t} + f_k^\mathrm{I}\frac{\partial \eta}{\partial t} + \frac{\partial q_{\mathrm{bx}k}}{\partial x} + \frac{\partial q_{\mathrm{by}k}}{\partial y} = 0 \quad k \in \{1, N-1\} \ , \tag{17}$$

219   and in the substrate (*Chavarrías et al.*, 2018):

$$\frac{\partial M_{sk}}{\partial t} - f_k^\mathrm{I}\frac{\partial \eta}{\partial t} = 0 \quad k \in \{1, N-1\} \ , \tag{18}$$

where $M_{ak} = F_{ak}L_a$ [m] and $M_{sk} = \int_{\eta_0}^{\eta_0+\eta-L_a} f_{sk}(z)\mathrm{d}z$ [m] are the volume of sediment of size

fraction k per unit of bed area in the active layer and the substrate, respectively. Parameter η_0 [m]

is a datum for bed elevation. Parameters $F_{ak} \in [0,1]$, $f_{sk} \in [0,1]$, and $f_k^{\mathrm{I}} \in [0,1]$ are the volume

fraction content of sediment of size fraction k in the active layer, substrate, and at the interface

between the active layer and the substrate, respectively. By definition, the sum of the volume

fraction content over all size fractions equals 1:

$$\sum_{k=1}^{N} F_{ak} = 1 \ , \quad \sum_{k=1}^{N} f_{sk}(z) = 1 \ , \quad \sum_{k=1}^{N} f_k^{\mathrm{I}} = 1 \ . \tag{19}$$

Under degradational conditions, the volume fraction content of size fraction k at the interface

between the active layer and the substrate is equal to that at the top part of the substrate ($f_k^{\mathrm{I}} =$

$f_{sk}(z = \eta - L_a)$ for $\partial\eta/\partial t < 0$). This allows for modelling of arbitrarily abrupt changes in grain

size due to erosion of previous deposits. Under aggradational conditions the sediment transferred

to the substrate is a weighted mixture of the sediment in the active layer and the bed load (*Parker*,

1991; *Hoey and Ferguson*, 1994; *Toro-Escobar et al.*, 1996). Here we simplify the analysis and we

assume that the contribution of the bed load to the depositional flux is negligible (i.e., $f_k^{\mathrm{I}} = F_{ak}$

for $\partial\eta/\partial t > 0$) (*Hirano*, 1971).

The magnitude of the sediment transport rate is assumed to be a function of the local bed shear

stress. We apply the sediment transport relation by *Engelund and Hansen* (1967) in a fractional

manner (*Blom et al.*, 2016, 2017) as well as the one by *Ashida and Michiue* (1971) (Appendix B).

The direction of the sediment transport (φ_{sk} [rad]) is affected by the secondary flow and the

bed slope (*Van Bendegom*, 1947):

$$\tan \varphi_{sk} = \frac{\sin \varphi_\tau - \frac{1}{g_{sk}}\frac{\partial\eta}{\partial y}}{\cos \varphi_\tau - \frac{1}{g_{sk}}\frac{\partial\eta}{\partial x}} \quad k \in \{1, N\} \ , \tag{20}$$

where g_{sk} [−] is a function that accounts for the influence of the bed slope on the sediment transport

direction and φ_τ [rad] is the direction of the sediment transport accounting for the secondary flow

only:

$$\tan \varphi_\tau = \frac{q_y - h\alpha_{\mathrm{I}}\frac{q_x}{Q}I}{q_x - h\alpha_{\mathrm{I}}\frac{q_y}{Q}I} \ . \tag{21}$$

Assuming a mild curvature, uniform flow conditions, and a logarithmic profile of the primary flow,

the constant α_{I} [−] is (*De Vriend*, 1977):

$$\alpha_{\mathrm{I}} = \frac{2}{\kappa^2}(1 - \alpha) \ . \tag{22}$$

The effect of the bed slope on the sediment transport direction depends on the grain size (*Parker*

250   *and Andrews*, 1985). We account for this effect setting:

$$g_{sk} = A_s \theta_k^{B_s} \quad k \in \{1, N\} \,, \tag{23}$$

252   where A_s $[-]$ and B_s $[-]$ are nondimensional parameters and θ_k $[-]$ is the *Shields* (1936) stress

253   (Appendix B). Different values of the coefficients A_s and B_s have been proposed (for a recent

254   review, see *Baar et al.* (2018)). We consider two possibilities: (1) $A_s = 1$, $B_s = 0$ (*Schielen et al.*,

255   1993) and (2) $A_s = 1.70$ and $B_s = 0.5$ (*Talmon et al.*, 1995). In the first and simpler case, the bed

256   slope effect is independent from the bed shear stress (*Engelund and Skovgaard*, 1973; *Engelund*,

257   1975). In the second, more complex, case, the bed slope effect is assumed to be dependent on

258   the fluid drag force on the grains, which is assumed to depend on the Shields stress (*Koch and*

259   *Flokstra*, 1981).

2.4   Linearised System of Equations

261   The system of equations describing the flow, change of bed level, and change of the bed surface

262   texture is highly non-linear. Here we linearise the system of equations to provide insight on the

263   fundamental properties of the model and to study the stability of perturbations. To this end we

264   consider a reference state that is a solution to the system of equations. The reference state is a

265   steady uniform straight flow in the x direction over an inclined plane bed composed of an arbitrary

266   number of size fractions. Mathematically: $h_0 = $ ct., $q_{x0} = $ ct., $q_{y0} = 0$, $I_0 = 0$, $\frac{\partial \eta}{\partial x} = $ ct. $= \frac{-C_f q_{x0}^2}{g h_0^3}$,

267   $\frac{\partial \eta}{\partial y} = 0$, $M_{ak0} = $ ct. $\forall k \in \{1, N-1\}$, where ct. denotes a constant different from 0 and subscript 0

268   indicates the reference solution.

269   We add a small perturbation to the reference solution denoted by $'$ and we linearise the resulting

270   system of equations. After substituting the reference solution we obtain a system of equations of

271   the perturbed variables:

$$\frac{\partial \mathbf{Q'}}{\partial t} + \mathbf{D_{x0}} \frac{\partial^2 \mathbf{Q'}}{\partial x^2} + \mathbf{D_{y0}} \frac{\partial^2 \mathbf{Q'}}{\partial y^2} + \mathbf{A_{x0}} \frac{\partial \mathbf{Q'}}{\partial x} + \mathbf{A_{y0}} \frac{\partial \mathbf{Q'}}{\partial y} + \mathbf{B_0} \mathbf{Q'} = 0 \,, \tag{24}$$

273   where the vector of dependent variables is:

$$\mathbf{Q'} = \left[h', q_x', q_y', I', \eta', [M_{ak}'] \right]^{\mathsf{T}} \,, \tag{25}$$

275   where the square bracket indicates the vector character.

276   The diffusive matrix in x direction is:

$$
\mathbf{D_{x0}} =
\left[
\begin{array}{ccccc:c}
0 & 0 & 0 & 0 & 0 & \mathbb{0} \\
2\nu\frac{q_{x0}}{h_0} & -2\nu & -\nu & 0 & 0 & \mathbb{0} \\
0 & 0 & -\nu & 0 & 0 & \mathbb{0} \\
0 & 0 & 0 & -\nu & 0 & \mathbb{0} \\
0 & 0 & 0 & 0 & 0 & \mathbb{0} \\
\hdashline
\mathbb{0} & \mathbb{0} & \mathbb{0} & \mathbb{0} & \mathbb{0} & \mathbb{0}
\end{array}
\right],
$$

277   (26)

278   where $\mathbb{0}$ denotes the zero matrix. The diffusive matrix in y direction is:

$$
\mathbf{D_{y0}} =
\left[
\begin{array}{ccccc:c}
0 & 0 & 0 & 0 & 0 & \mathbb{0} \\
\nu\frac{q_{x0}}{h_0} & -\nu & 0 & 0 & 0 & \mathbb{0} \\
\nu\frac{q_{x0}}{h_0} & -\nu & -2\nu & 0 & 0 & \mathbb{0} \\
0 & 0 & 0 & -\nu & 0 & \mathbb{0} \\
0 & 0 & 0 & 0 & \left.\frac{\partial q_{by}}{\partial\frac{\partial\eta}{\partial y}}\right|_0 & \mathbb{0} \\
\hdashline
\mathbb{0} & \mathbb{0} & \mathbb{0} & \mathbb{0} & \left[\left.\frac{\partial q_{byk}}{\partial\frac{\partial\eta}{\partial y}}\right|_0 - f^{\mathrm{I}}_{k0}\left.\frac{\partial q_{by}}{\partial\frac{\partial\eta}{\partial y}}\right|_0\right] & \mathbb{0}
\end{array}
\right].
$$

279   (27)

280   The advective matrix in x direction is:

$$
\mathbf{A_{x0}} =
\left[
\begin{array}{ccccc:c}
0 & 1 & 0 & 0 & 0 & \mathbb{0} \\
gh_0 - \left(\frac{q_{x0}}{h_0}\right)^2 & 2\frac{q_{x0}}{h_0} & 0 & 0 & gh_0 & \mathbb{0} \\
0 & 0 & \frac{q_{x0}}{h_0} & -\beta^* q_{x0} & 0 & \mathbb{0} \\
0 & 0 & -\frac{q_{x0}}{h_0^2 L_{\mathrm{I}}^*} & \frac{q_{x0}}{h_0} & 0 & \mathbb{0} \\
\left.\frac{-q_{x0}}{h_0}\frac{\partial q_{bx}}{\partial q_x}\right|_0 & \left.\frac{\partial q_{bx}}{\partial q_x}\right|_0 & 0 & 0 & 0 & \left[\left.\frac{\partial q_{bx}}{\partial M_{al}}\right|_0\right] \\
\hdashline
\left[\left.\frac{-q_{x0}}{h_0}\frac{\partial q_{bk}}{\partial q_x}\right|_0 + f^{\mathrm{I}}_{k0}\left.\frac{q_{x0}}{h_0}\frac{\partial q_b}{\partial q_x}\right|_0\right] & \left[\left.\frac{\partial q_{bxk}}{\partial q_x}\right|_0 - f^{\mathrm{I}}_{k0}\left.\frac{\partial q_{bx}}{\partial q_x}\right|_0\right] & \mathbb{0} & \mathbb{0} & \mathbb{0} & \left[\left.\frac{\partial q_{bxk}}{\partial M_{al}}\right|_0 - f^{\mathrm{I}}_{k0}\left.\frac{\partial q_{bx}}{\partial M_{al}}\right|_0\right]
\end{array}
\right].
$$

281   (28)

282   The advective matrix in y direction is:

$$
\mathbf{A_{y0}} =
\left[
\begin{array}{ccccc:c}
0 & 0 & 1 & 0 & 0 & \mathbb{0} \\
0 & 0 & \frac{q_{x0}}{h_0} & -\beta^* q_{x0} & 0 & \mathbb{0} \\
gh_0 & 0 & 0 & 0 & gh_0 & \mathbb{0} \\
0 & 0 & 0 & 0 & 0 & \mathbb{0} \\
0 & 0 & \left.\frac{\partial q_{by}}{\partial q_y}\right|_0 & \left.\frac{\partial q_{by}}{\partial I}\right|_0 & 0 & \mathbb{0} \\
\hdashline
\mathbb{0} & \mathbb{0} & \left[\left.\frac{\partial q_{byk}}{\partial q_y}\right|_0 - f^{\mathrm{I}}_{k0}\left.\frac{\partial q_{by}}{\partial q_y}\right|_0\right] & \left[\left.\frac{\partial q_{byk}}{\partial I}\right|_0 - f^{\mathrm{I}}_{k0}\left.\frac{\partial q_{by}}{\partial I}\right|_0\right] & \mathbb{0} & \mathbb{0}
\end{array}
\right].
$$

283   (29)

284   The matrix of linear terms is:

$$
\mathbf{B_0} =
\left[
\begin{array}{ccccc:c}
0 & 0 & 0 & 0 & 0 & \mathbb{0} \\
\dfrac{-3C_\mathrm{f}q_\mathrm{x0}^2}{h_0^3} & \dfrac{2C_\mathrm{f}q_\mathrm{x0}}{h_0^2} & 0 & 0 & 0 & \mathbb{0} \\
0 & 0 & \dfrac{C_\mathrm{f}q_\mathrm{x0}}{h_0^2} & 0 & 0 & \mathbb{0} \\
0 & 0 & 0 & \dfrac{q_\mathrm{x0}}{h_0^2 L_\mathrm{I}^*} & 0 & \mathbb{0} \\
0 & 0 & 0 & 0 & 0 & \mathbb{0} \\
\hdashline
\mathbb{0} & \mathbb{0} & \mathbb{0} & \mathbb{0} & \mathbb{0} & \mathbb{0}
\end{array}
\right] .
$$

285   (30)

286   We assume that the perturbations can be represented as a Fourier series, which implies that

287   they are piecewise smooth and bounded for $x = \pm\infty$. Using this assumption the solution of the

288   perturbed system is expressed in the form of normal modes:

$$
\mathbf{Q}' = \mathrm{Re}\left(\mathbf{V}\mathrm{e}^{\mathrm{i}(k_\mathrm{wx} + k_\mathrm{wy} - \omega t)}\right) ,
$$

289   (31)

290   where i is the imaginary unit, k_wx [rad/m] and k_wy [rad/m] are the real wave numbers in x and

291   y direction, respectively, $\omega = \omega_\mathrm{r} + \mathrm{i}\omega_\mathrm{i}$ [rad/s] is the complex angular frequency, $\mathbf{V}$ is the complex

292   amplitude vector, and Re denotes the real part of the solution (which we will omit in the subsequent

293   steps). The variable ω_r is the angular frequency and ω_i the attenuation coefficient. A value of $\omega_\mathrm{i} > 0$

294   implies growth of perturbations and $\omega_\mathrm{i} < 0$ decay. Substitution of equation (31) in equation (24)

295   yields:

$$
\left[\mathbf{M_0} - \omega\mathbb{1}\right]\mathbf{V} = 0 ,
$$

296   (32)

297   where:

$$
\mathbf{M_0} = \mathbf{D_{x0}}k_\mathrm{wx}^2\mathrm{i} + \mathbf{D_{y0}}k_\mathrm{wy}^2\mathrm{i} + \mathbf{A_{x0}}k_\mathrm{wx} + \mathbf{A_{y0}}k_\mathrm{wy} - \mathbf{B_0}\mathrm{i} ,
$$

298   (33)

299   and $\mathbb{1}$ denotes the unit matrix. Equation (32) is an eigenvalue problem in which the eigenvalues

300   of $\mathbf{M_0}$ (as a function of the wave number) are the values of ω satisfying equation (32).

301   The solution of the linear model provides information regarding the development of small

302   amplitude oscillations only, but for an arbitrary wave number. For this reason the linear model

303   is convenient for studying the well-posedness of the model, which we will assess in the following

304   section.

3 Instability, Hyperbolicity, and Ill-Posedness

Ill-posedness has been related to the system of governing equations losing its hyperbolic charac-
ter. Stability analysis investigates growth and decay of perturbations of a base state. The two
mathematical problems may seem unrelated but in fact they are strongly linked. In this section
we clarify the terms unstable, hyperbolic, and ill-posed, and present the mathematical framework
that we use to study the well-posedness of the system of equations.

A system is stable if perturbations to an equilibrium state decay and the solution returns to its
original state. This is equivalent to saying that all possible combinations of wave numbers in the x
and y directions yield a negative growth rate (ω_i, equation (31)). An example of a stable system in
hydrodynamics is the inviscid Shallow Water Equations (iSWE) for a Froude number smaller than
2 (*Jeffreys*, 1925; *Balmforth and Mandre*, 2004; *Colombini and Stocchino*, 2005). In figure 1a we
show the maximum growth rate of perturbations to a reference solution (Case I1, tables 1 and 2)
of the iSWE on an inclined plane (i.e., the first 3 equations of the complete system, equation (24),
with neither secondary flow nor diffusion). The growth rate is obtained numerically by computing
the eigenvalues of the reduced matrix $\mathbf{M_0}$ (the first 3 rows and columns in equation (33)) for
wave numbers between 0 and $250\,\mathrm{rad/m}$, which is equivalent to wavelengths ($l_{\mathrm{wx}} = 2\pi/k_{\mathrm{wx}}$ and
equivalently for y) down to $1\,\mathrm{cm}$. Figure 1b presents the same information as figure 1a in terms
of wavelength rather than wave number to better illustrate the behaviour for large wavelengths.
The growth rate is negative for all wave numbers, which confirms that the iSWE for Fr < 2 yield
a stable solution.

u [m/s]	v [m/s]	h [m]	C_f [$-$]
1	0	1	0.007

Table 1: Reference state.

Case	model	Fr	stability	mathematical character
I1	iSWE	0.32	stable	well-posed
B1	iSWE+Exner	0.32	unstable	well-posed
I2	iSWE	2.01	unstable	ill-posed

Table 2: Cases of a stable well-posed model (I1), an unstable well-posed model (B1), and an ill-
posed model (I2). Case I2 has the same parameter values as Case I1 but for the mean flow velocity
which is equal to $6.30\,\mathrm{m/s}$.

A system is unstable when perturbations to an equilibrium state grow and the solution diverges
from the initial equilibrium state. The growth of river bars is an example of an unstable system in
river morphodynamics. A straight alluvial channel is stable if the width-to-depth ratio is sufficiently
small and, above a certain threshold value, the channel becomes unstable and free alternate bars
grow (*Engelund and Skovgaard*, 1973; *Fredsøe*, 1978; *Colombini et al.*, 1987; *Schielen et al.*, 1993).

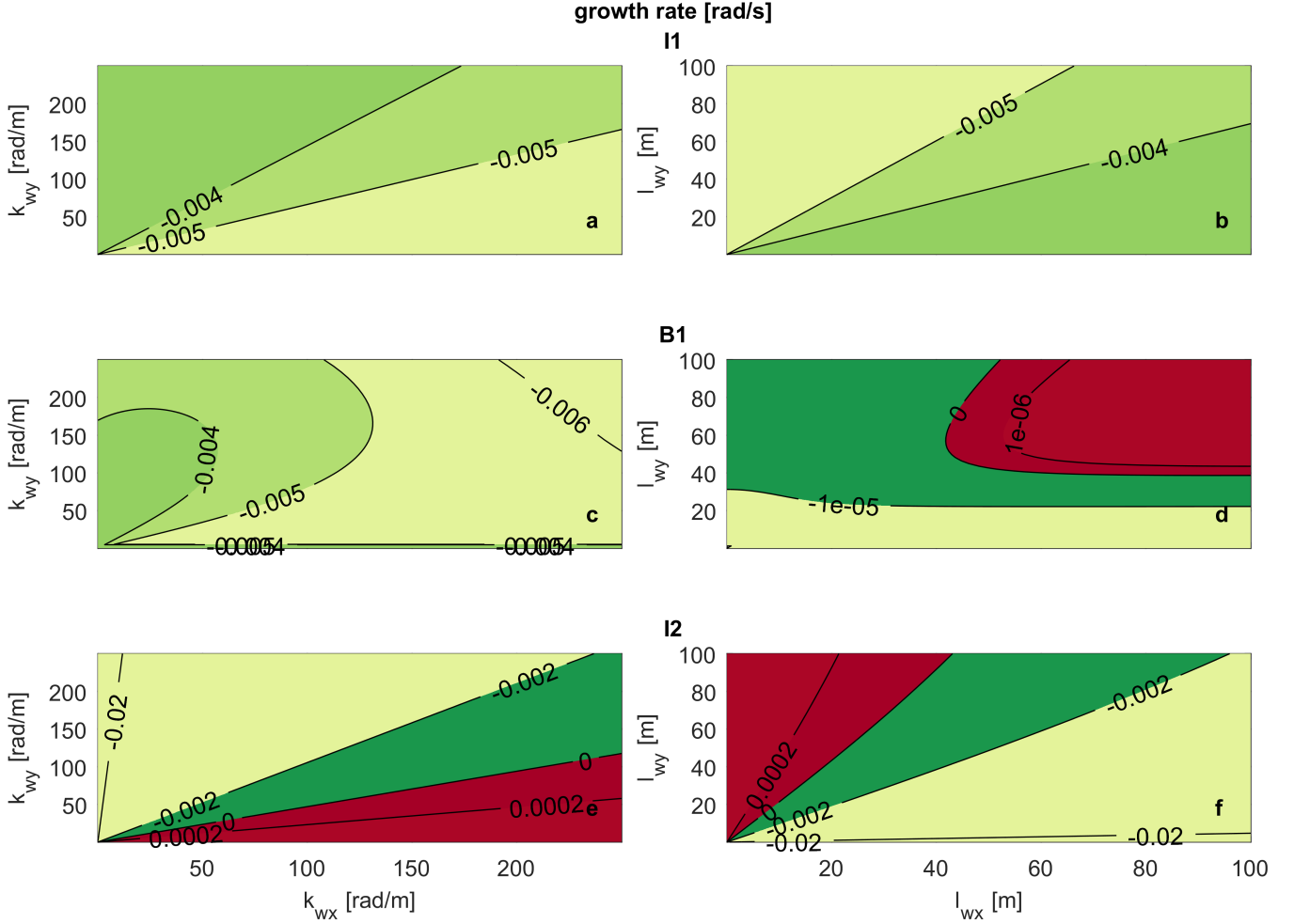Figure 1: Growth rate of perturbations added to the reference case (tables 1 and 2) as a function of the wave number and the wavelength: (**a**)-(**b**) iSWE, Fr < 2 (Case I1, well-posed), (**c**)-(**d**) iSHE+Exner (Case B1, well-posed), and (**e**)-(**f**) iSWE, Fr > 2 (Case I2, ill-posed). The subplots in the two columns show the same information but highlight the behaviour for large wave numbers (left column) and for large wavelengths (right column). Red and green indicates growth and decay of perturbations, respectively.

Mathematically, an unstable system has a region, a domain in the wave number space, in which the growth rate of perturbations is positive. In figure 1c-d we present the growth rate of perturbations to a reference solution consisting of uniform flow (table 1) on an alluvial bed composed of unisize sediment with a characteristic grain size equal to $0.001\,\text{m}$ (Case B1, table 2). The sediment transport rate is computed using the relation by *Engelund and Hansen* (1967) (equation (42)) and the effect of the bed slope on the sediment transport direction is accounted for using the simplest formulation, $g_{\text{s}} = 1$. Figure 1d confirms the classical result of linear bar theory: there exists a critical transverse wavelength (l_{wyc}) below which all perturbations decay. In our particular case $l_{\text{wyc}} = 40.2\,\text{m}$. Impermeable boundary conditions at the river banks limit the possible wavelengths to fractions of the channel width B [m] such that $l_{\text{wy}} = 2B/m$ for $m = 1, 2, ...$ (*Callander*, 1969). As the most unstable mode is the first one (i.e., $m = 1$, alternate bars) (*Colombini et al.*, 1987; *Schielen et al.*, 1993), the minimum channel width above which perturbations grow is $B_{\text{c}} = l_{\text{wyc}}/2 = 20.1\,\text{m}$,

which confirms the results of *Schielen et al.* (1993). Figure 1c highlights, as for case I1, the decay of short waves.

A particular case of instability is that in which the domain of positive growth rate extends to infinitely large wave numbers (i.e., short waves). Under this condition there is no cutoff wave number above which we can neglect the contribution of ever shorter waves with non-zero growth rates. For any unstable perturbation a shorter one can be found which is even more unstable. This implies that the growth rate of an infinitesimal perturbation (i.e., noise) tends to infinity. Such a system cannot represent a physical phenomenon, as the growth rate of any physical process in nature is bounded. A system in which the growth rate of infinitesimal perturbations tends to infinity does not have a unique solution depending continuously on the initial and boundary conditions, which implies that the system is ill-posed (*Hadamard*, 1923; *Joseph and Saut*, 1990). An example of an ill-posed hydrodynamic model is the iSWE for flow with a Froude number larger than 2. In figure 1e-f we show the growth rate of perturbations to the reference solution of a case in which the Froude number is slightly larger than 2 (Case I2, table 2). The growth rate extends to infinitely large wave numbers, which confirms that this case is ill-posed. A model being ill-posed is an indication that there is a relevant physical mechanism that has been neglected in the model derivation (*Fowler*, 1997). Viscous forces regularise the iSWE (i.e., make the model well-posed) and rather than ill-posed, the viscous Shallow Water Equations become simply unstable for a Froude number larger than 2, predicting the formation of roll-waves (*Balmforth and Mandre*, 2004; *Balmforth and Vakil*, 2012; *Rodrigues and Zumbrun*, 2016; *Barker et al.*, 2017a,b).

Chaotic models, just as ill-posed models, are sensitive to the initial and boundary conditions and lose their predictive capabilities in a deterministic sense (*Lorenz*, 1963). Yet, there are two essential differences. First, chaotic systems lose their predictive capabilities after a certain time (*Devaney*, 1989; *Banks et al.*, 1992), yet there exists a finite time in which the dynamics are predictable. In ill-posed models infinitesimal perturbations to the initial condition cause a finite divergence in the solution in an arbitrarily (but fixed) short time. Second, while the dynamics of a chaotic model are not predictable in deterministic terms after a certain time, these continue to be predictable in statistical terms. For this reason, although being sensitive to the initial and boundary conditions, a model presenting chaotic properties can be used, for instance, to capture the essential dynamics and spatio-temporal features of river braiding (*Murray and Paola*, 1994, 1997). On the contrary, the dynamics of an ill-posed model cannot be analysed in statistical terms.

The numerical solution of an ill-posed problem continues to change as the grid is refined because a smaller grid size resolves larger wave numbers with faster growth rates (*Joseph and Saut*, 1990; *Kabanikhin*, 2008; *Barker et al.*, 2015; *Woodhouse et al.*, 2012). In other words, the numerical solution of an ill-posed problem does not converge when the grid cell size is reduced. This property emphasizes the unrealistic nature of ill-posed problems and shows that ill-posed models cannot be applied in practice.

We present an example of grid dependence specifically related to river morphodynamics under conditions with mixed-size sediment. We consider a case of degradation into a substrate finer than the active layer, as this is a situation in which the active layer model is prone to be ill-posed (Section 1). The reference state is the same as in Case B1, yet the sediment is a mixture of two sizes equal to 0.001 m and 0.010 m. The bed surface is composed of 10 % of fine sediment. The active layer thickness is equal to 0.05 m, which in this case is representative of small dunes covering the bed (e.g. *Deigaard and Fredsøe*, 1978; *Armanini and Di Silvio*, 1988; *Blom*, 2008). Depending on the substrate composition, this situation yields an ill-posed model (*Chavarrías et al.*, 2018). When the substrate is composed of 50 % of fine sediment (Case H1, table 3), the problem is well-posed and it is ill-posed when the substrate is composed of 90 % of fine sediment (Case H2, table 3).

We use the software package Delft3D (*Lesser et al.*, 2004) to solve the system of equations. We stress that the problem of ill-posedness is inherent to the system of equations and independent from the numerical solver. We have implemented a subroutine that assesses the well-posedness of the system of equations at each node and time step. The domain is 100 m long and 10 m wide. The downstream water level is lowered at a rate of 0.01 m/h to induce degradational conditions. The upstream sediment load is constant and equal to the equilibrium value of the reference state (*Blom et al.*, 2017). The cells are square and we consider three different sizes (table 3). The time step varies between simulations to maintain a constant value of the CFL number.

Case	f_1^{I} $[-]$	Δx [m]	mathematical character
H1a	0.5	0.50	well-posed
H1b	0.5	0.25	well-posed
H1c	0.5	0.10	well-posed
H2a	0.9	0.50	ill-posed
H2b	0.9	0.25	ill-posed
H2c	0.9	0.10	ill-posed

Table 3: Cases showing the effect of grid cell size on the numerical solution of well-posed and ill-posed models.

Figure 2 presents the bed elevation after 10 h. The result of the well-posed case (H1, left column) is grid independent. The result of the ill-posed case (H2, right column) changes as the grid is refined and presents an oscillatory pattern characteristic of ill-posed simulations (*Joseph and Saut*, 1990; *Woodhouse et al.*, 2012; *Barker et al.*, 2015; *Chavarrías et al.*, 2018). The bed seems to be flat in the ill-posed simulation with a coarser grid (figure 2b). This is because oscillations grow slowly on a coarse grid and require more time to be perceptible. The waviness of the bed is seen in the result of the check routine, as it predicts ill-posedness only at those locations where the bed degrades (the stoss face of the oscillations). The fact that the model is well-posed in almost the entire domain in the ill-posed case solved using a cell sizes equal to 0.25 m (H2b, figure 2d) and 0.10 m (H2c, figure 2f) does not mean that the results are realistic. Non-physical oscillations have grown and vertically mixed the sediment such that the situation is well-posed after 10 h (*Chavarrías*

408   *et al.*, 2018). We provide a movie of figure 2 in the online supplementary material.
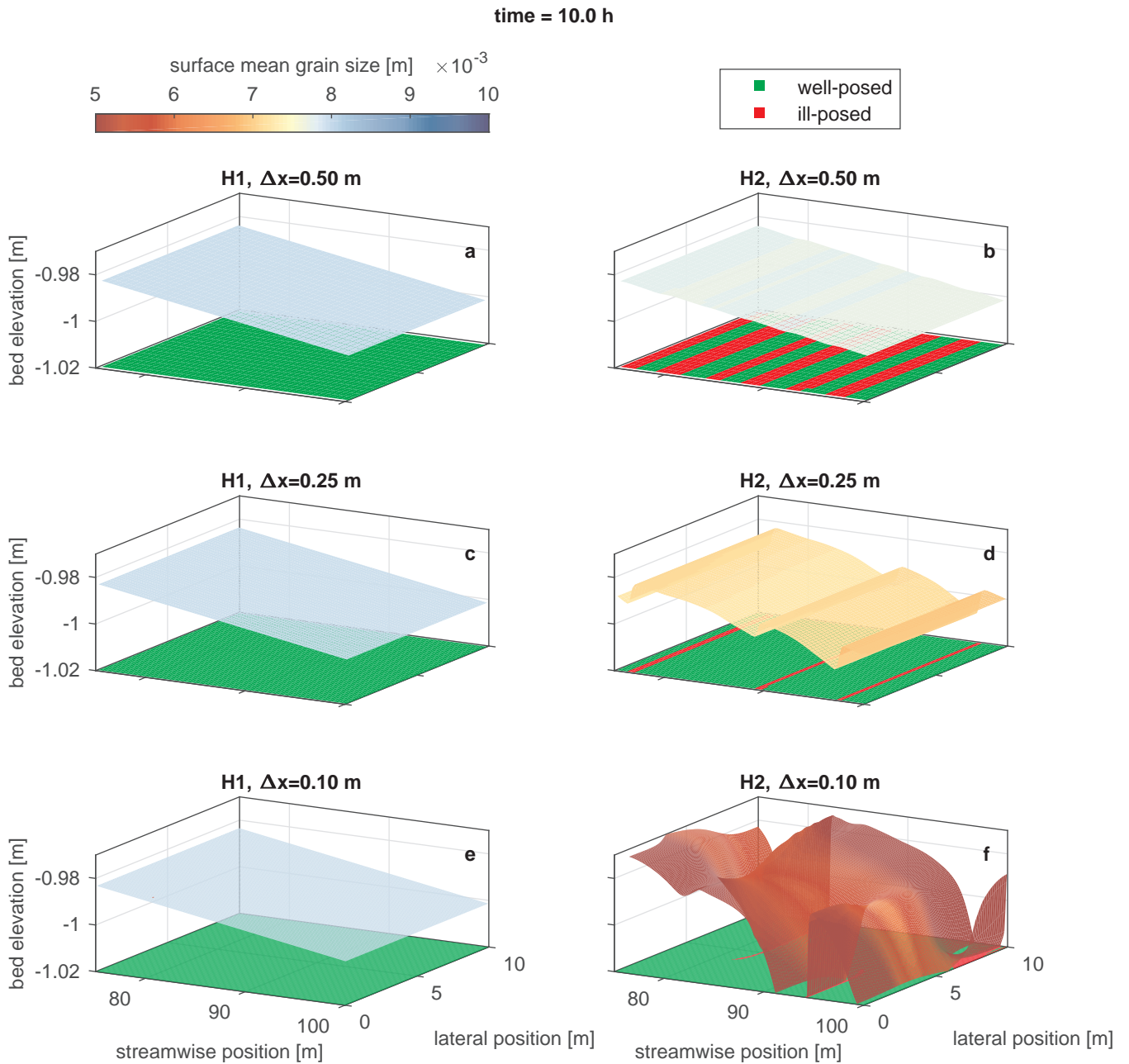

Figure 2: Simulated bed elevation (surface) and mean grain size at the bed surface (colour) of a well-posed case (left column, H1, table 3) and an ill-posed case (right column, H2, table 3). In each row we present the results for varying cell size. The colour of the $x-y$ plane shows the result of the routine that checks whether the conditions at each node yield a well-posed (green) or an ill-posed (red) model.

409   In the above idealised situations it is evident that the oscillations are non-physical and it is

410 straightforward to do a converge test to clarify that the solution is grid dependent. In complex

411 domains in which several processes play a role, it is more difficult to associate oscillations to

412 ill-posedness. Moreover, in long term applications the growth rate of perturbations may be fast

413 compared to the frequency at which model results are assessed, which may hide the consequences

of ill-posedness. If one studies a process that covers months or years (and consequently analyses the results on a monthly basis) but perturbations due to ill-posedness grow on an hourly scale, it may be difficult to identify that the problem is ill-posed. Using poor numerical techniques to solve the system of equations also contributes to hiding the consequences of ill-posedness as numerical diffusion dampens perturbations. These factors may explain why the problem of ill-posedness in mixed-sediment river morphodynamics is not widely acknowledged.

In the river morphodynamics community, the term ellipticity has been used to refer to ill-posedness of the system of equations in contrast to hyperbolicity, which is associated to well-posedness (*Ribberink*, 1987; *Mosselman*, 2005; *Stecca et al.*, 2014; *Siviglia et al.*, 2017; *Chavarrías et al.*, 2018). In general the terms are equivalent, but not always. We consider a unit vector $\hat{n}$ in the direction (x, y), $\hat{n} = (\hat{n_x}, \hat{n_y})$. The system of equations (24) is hyperbolic if matrix $\mathbf{A} = \mathbf{A_{x0}}\hat{n_x} + \mathbf{A_{y0}}\hat{n_y}$ diagonalises with real eigenvalues $\forall \hat{n}$ (e.g. *LeVeque*, 2004; *Castro et al.*, 2009). Neglecting friction and diffusive processes (i.e., $\mathbf{B_0} = \mathbf{D_{x0}} = \mathbf{D_{y0}} = \mathbb{0}$), hyperbolicity implies that the eigenvalues of $\mathbf{M_0}$ (equation (33)) are real. In this case, as the growth rate of perturbations (i.e., the imaginary part of the eigenvalues of $\mathbf{M_0}$) is equal to 0 regardless of the wave number, the system of equations is well-posed. As the coefficients of $\mathbf{A}$ are real, complex eigenvalues appear in conjugate pairs. This means that if $\mathbf{A}$ has a complex eigenvalue (i.e., the problem is not hyperbolic), at least one wave will have a positive growth rate. Neglecting friction and diffusive processes, non-hyperbolicity implies that infinitely large wave numbers have a positive growth rate. We conclude that, in the absence of diffusion and friction, lack of hyperbolicity implies ill-posedness. Note that ellipticity (i.e., the eigenvalues of $\mathbf{A}$ are all complex) is not required for the problem to be ill-posed, as it suffices that the problem is not hyperbolic. When considering diffusion and friction even when $\mathbf{A}$ has complex eigenvalues, the imaginary part of the eigenvalues of $\mathbf{M_0}$ may all be negative and the problem well-posed.

Finally, well-posedness and hyperbolicity are similar terms when dealing with problems arising from conservation laws and changes with time, as hyperbolicity guarantees the existence of wave solutions (*Lax*, 1980; *Courant and Hilbert*, 1989; *Strikwerda*, 2004; *Toro*, 2009; *Dafermos*, 2010; *Bressan*, 2011; *Dafermos*, 2016). In communities such as materials science, it is the term hyperbolicity that is associated to ill-posedness, as a smooth solution of, for instance the stress, requires that the system is elliptic (*Knowles and Sternberg*, 1975, 1976; *Veprek et al.*, 2007).

4   Stability Analysis

In this section we study the applicability of the system of equations to model two-dimensional river morphodynamics by means of a stability analysis of perturbations. We study the effects of the secondary flow model (Sections 4.1) and the bed slope (Section 4.2) on model ill-posedness.

4.1 Ill-Posedness Due to Secondary Flow

In this section we study how the stability of the system of equations is affected by the secondary flow model. To gain insight we compare three cases. In the first case we omit secondary flow. In the second and third cases we include the secondary flow model with and without considering diffusion (table 4).

Case	secondary flow	ν	stability	mathematical character
S1	no	ν_{E}	stable	well-posed
S2	yes	ν_{E}	unstable	well-posed
S3	yes	0	unstable	ill-posed

Table 4: Variations to the reference state (table 1) and results of the linear analysis with respect to secondary flow.

The first case is equivalent to I1 (table 2), yet the eddy viscosity is equal to the value derived by *Elder* (equation (4), $\nu = \nu_{\mathrm{E}} = 0.0057\,\mathrm{m^2/s}$). In figure 3a-b we plot the maximum growth rate of perturbations as a function of the wave number and the wavelength, respectively. Diffusion appears to significantly dampen perturbations (compare figure 1a in which diffusion is neglected to figure 3a).

In the second case we repeat the analysis including the equation for advection and diffusion of the secondary flow intensity (i.e., the first 4 rows and columns of matrix $\mathbf{M_0}$ in equation (33), Case S2, table 4). We observe that accounting for secondary flow introduces an instability mechanism (figure 3d). For the specific conditions of the case, a growth domain appears for wavelengths between $0.7\,\mathrm{m}$ and $39\,\mathrm{m}$ long and between $0.4\,\mathrm{m}$ and $19\,\mathrm{m}$ wide. The maximum growth corresponds to a wavelength in the x and y direction equal to $1.29\,\mathrm{m}$ and $0.74\,\mathrm{m}$, respectively. This situation is well-posed, as for large wave numbers perturbations decay (figure 3c). Yet, the model is unsuitable for reproducing such instability, as it predicts growth of perturbations with a length scale of the order of the flow depth and shorter, for which the SWE model is not suited. Given the fact that we consider a depth-averaged formulation of the primary flow, processes that scale with the flow depth are not resolved by the model and consequently perturbations at that scale must decay to yield physically realistic results. Otherwise, scales of the order of the flow depth become relevant, which contradicts the assumptions of the depth-averaged formulation. To model processes that scale with the flow depth such as dune growth, it is necessary to account for non-depth-averaged flow formulations that consider, for instance, rotational flow (*Colombini and Stocchino*, 2011, 2012), or non-hydrostatic pressure (*Giri and Shimizu*, 2006; *Shimizu et al.*, 2009).

In the third case we test the secondary flow model without accounting for diffusion in the system of equations ($\nu = 0$, Case S3, table 4). We observe that the instability domain extends to infinitely large wave numbers (figure 3e), which implies that this model is ill-posed (Section 3). We now aim to prove that the Shallow Water Equations in combination with the secondary flow model without
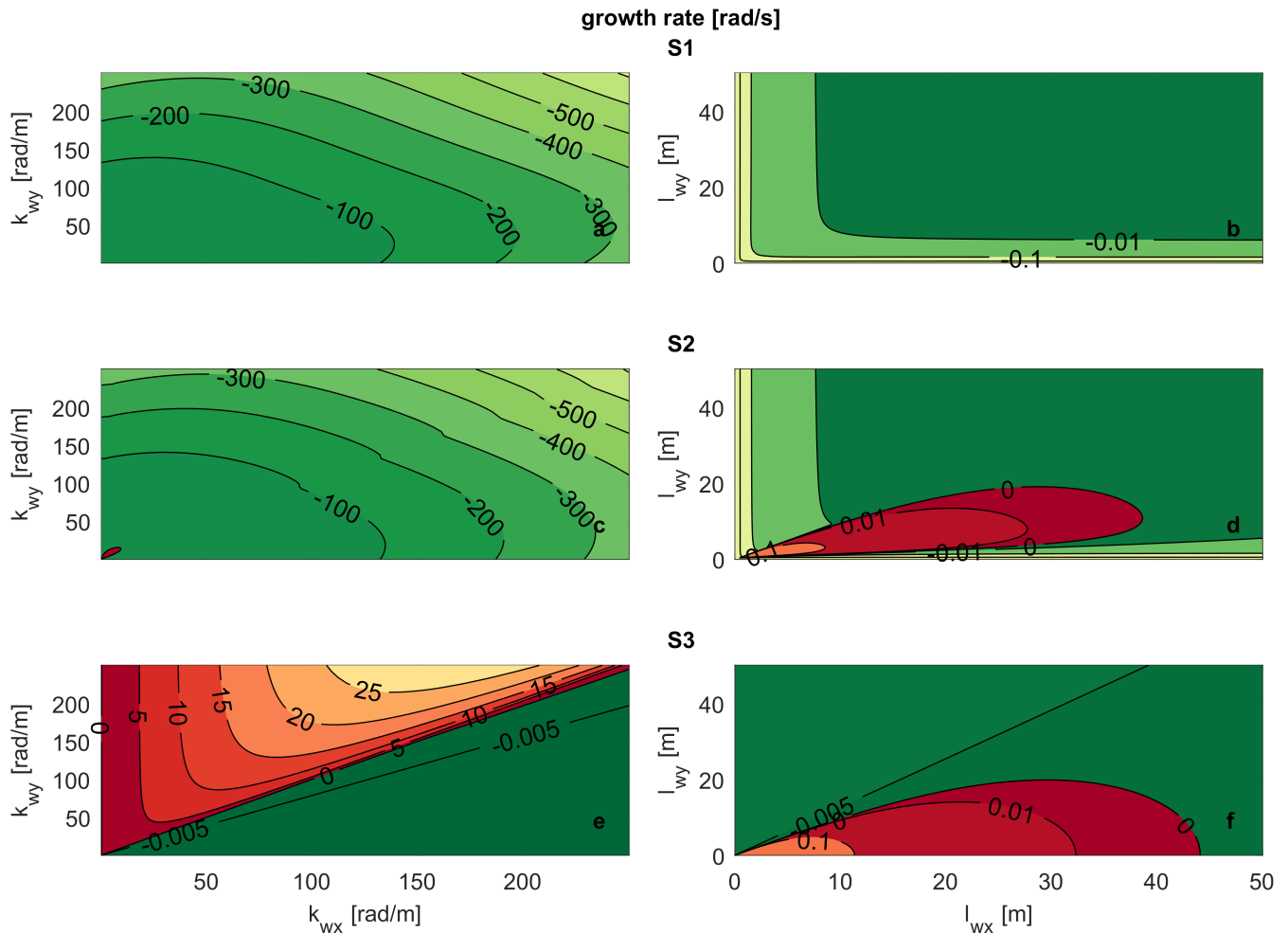
Figure 3: Growth rate of perturbations added to the reference case (tables 1 and 4) as a function of the wave number and the wavelength: (**a**)-(**b**) without secondary flow (Case S1, well-posed), (**c**)-(**d**) accounting for secondary flow with diffusion (Case S2, well-posed), and (**e**)-(**f**) accounting for secondary flow without diffusion (Case S3, ill-posed). The subplots in the two columns show the same information but highlight the behaviour for large wave numbers (left column) and for large wavelengths (right column). Red and green indicates growth and decay of perturbations, respectively.

478   diffusion always yields an ill-posed model. To this end we obtain the characteristic polynomial

479   of matrix $\mathbf{M_0}$ (equation (33)). We compute the discriminant of the fourth order characteristic

480   polynomial and we find that for $k_{wx} < k_{wy}$ the growth rate of perturbations is positive (Appendix

481   C). The model is ill-posed, as there always exists a domain of growth extending to infinitely large

482   wave numbers in the transverse direction.

483   We assess how the length scale of the instability related to the secondary flow model depends

484   on the flow parameters. For this purpose we compute the shortest wave with positive growth

485   for a varying diffusion coefficient and flow conditions (figure 4). We observe that, independently

486   from the flow conditions, the theoretical value of the diffusion coefficient derived by *Elder* (1959)

487   (equation (4)) is insufficient for dampening oscillations scaling with the flow depth. We conclude

488   that if the diffusion coefficient is realistic, the treatment of the secondary flow yields an unrealistic

489   model. It is necessary to use an unrealistically large value of the diffusion coefficient to obtain a

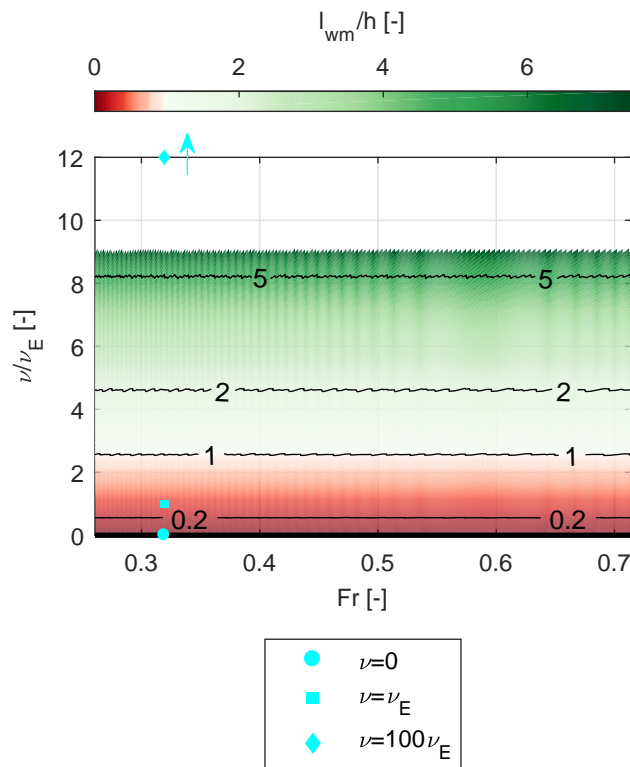490   realistic depth-averaged model in which perturbations scaling with the flow depth decay.

Figure 4: Wavelength of the shortest perturbation with positive growth rate (l_{wm}) relative to the flow depth (h) as a function of the Froude number (Fr) and the diffusion coefficient (ν) relative to the diffusion coefficient according to *Elder* (1959) (ν_{E}). Different flow conditions are studied varying the flow depth between $0.2\,\mathrm{m}$ and $1.5\,\mathrm{m}$ from the reference case (table 1). The cyan markers indicate the conditions of three numerical simulations with different values of the diffusion coefficient (Section 5.1). The arrow next to the diamond marker indicates that the value lies outside the figure. Red (green) colours indicate that the shortest wave length with positive growth rate are smaller (larger) than the flow depth.

4.2   Ill-Posedness Due to Bed Slope Effect

492   In this section we study the influence of considering the effect of the bed slope on model well-

493   posedness. To gain insight we compare 5 cases in which we consider unisize and mixed-size sedi-

494   ment, various sediment transport relations, and various bed slope functions (table 5). We neglect

495   secondary flow and diffusion to reduce the complexity of the problem (*Parker*, 1976; *Fredsøe*, 1978;

496   *Colombini et al.*, 1987; *Schielen et al.*, 1993).

497   Our reference case is B1 (Section 3) which considers unisize sediment conditions, and the

498   effect of the bed slope on the sediment transport direction is accounted for using the simplest

499   formulation, $g_{\mathrm{s}} = 1$. We have shown that this case is well-posed. Neglecting the effect of the bed

500   slope on the sediment transport direction (Case B2, table 5) makes the problem ill-posed (figure

501   5a). This illustrates that accounting for the effect of the bed slope is required for obtaining not

502   only physically realistic but also mathematically well-posed results. We prove that the Shallow

503   Water Equations in combination with the *Exner* (1920) equation without considering the effect of

504   the bed slope always yields an ill-posed model by studying the growth rate of perturbations in the

505   limit for the wave number k_{wy} tending to infinity (Appendix D).

Case	sediment	d_2 [m]	sed. trans.	bed slope	mathematical character
B1	unisize	-	EH	$g_s = 1$	well-posed
B2	unisize	-	EH	No	ill-posed
B3	mixed-size	0.004	AM	$g_{sk} = 1$	well-posed
B4	mixed-size	0.004	AM	$g_{sk} = 1.7\theta_k^{0.5}$	ill-posed
B5	mixed-size	0.012	AM	$g_{sk} = 1$	ill-posed

Table 5: Variations to the reference state (table 1) and results of the linear analysis with respect to the effect of the bed slope on the sediment transport direction. EH and AM refer to the sediment transport relations by *Engelund and Hansen* (1967) and *Ashida and Michiue* (1971), respectively.

506   The fact that the bed slope effect dampens perturbations under unisize conditions is expected

507   from the fact that the only diffusive term in the system of equations is $\partial q_{by}/\partial s_y$ (equation (27)),

508   where $s_y = \partial \eta/\partial y$. This term is negative and approximately equal to $-q_b/g_s$ for a small streamwise

509   slope. When we consider more than one grain size, diffusive terms appear in each active layer

510   equation. We find that these diffusive terms may be positive, which hints at the possibility of an

511   antidiffusive behaviour, which may lead to ill-posedness. To study this possibility we compute the

512   growth rate of perturbations of a simplified case consisting of two sediment size fractions. In the

513   limit for the wave numbers tending to infinity, the maximum growth rate is:

$$\omega_i^{lim} = \alpha_1 \left(r_{y1} - d_{x1,1} \right)^2 + \alpha_2 \left(r_{y1} - d_{x1,1} \right) + \alpha_3 \, , \tag{34}$$

515   where α_i for $i = 1, 2, 3$ are parameters relating the flow and the sediment transport rate (Appendix

516   E). The parameter r_{y1} explains how the sediment transport rate of the fine fraction is affected by

517   changes in the transverse bed slope:

$$r_{y1} = \frac{\partial q_{by1}/\partial s_y}{\partial q_{by}/\partial s_y} \, , \tag{35}$$

519   and the parameter $d_{x1,1}$ relates changes in the sediment transport rate to changes in the volume

520   of sediment in the active layer:

$$d_{x1,1} = \frac{\partial q_{bx1}/\partial M_{a1}}{\partial q_{bx}/\partial M_{a1}} \, . \tag{36}$$

522   As $\alpha_1 > 0$ (Appendix E), there exist an interval $\left(r_{y1} - d_{x1,1} \right)^- < \left(r_{y1} - d_{x1,1} \right) < \left(r_{y1} - d_{x1,1} \right)^+$ in

523   which $\omega_i^{lim} < 0$ and the model is well-posed. Outside the interval, $\omega_i^{lim} > 0$ and the problem is

524   ill-posed.

525   The physical interpretation of the limit values for obtaining a well-posed model is as follows.

526   The effect of the transverse bed slope (r_{y1}) needs to be balanced with respect to the effect of

527   changes in surface texture ($d_{x1,1}$) to obtain a well-posed model. For a given $d_{x1,1}$, if parameter
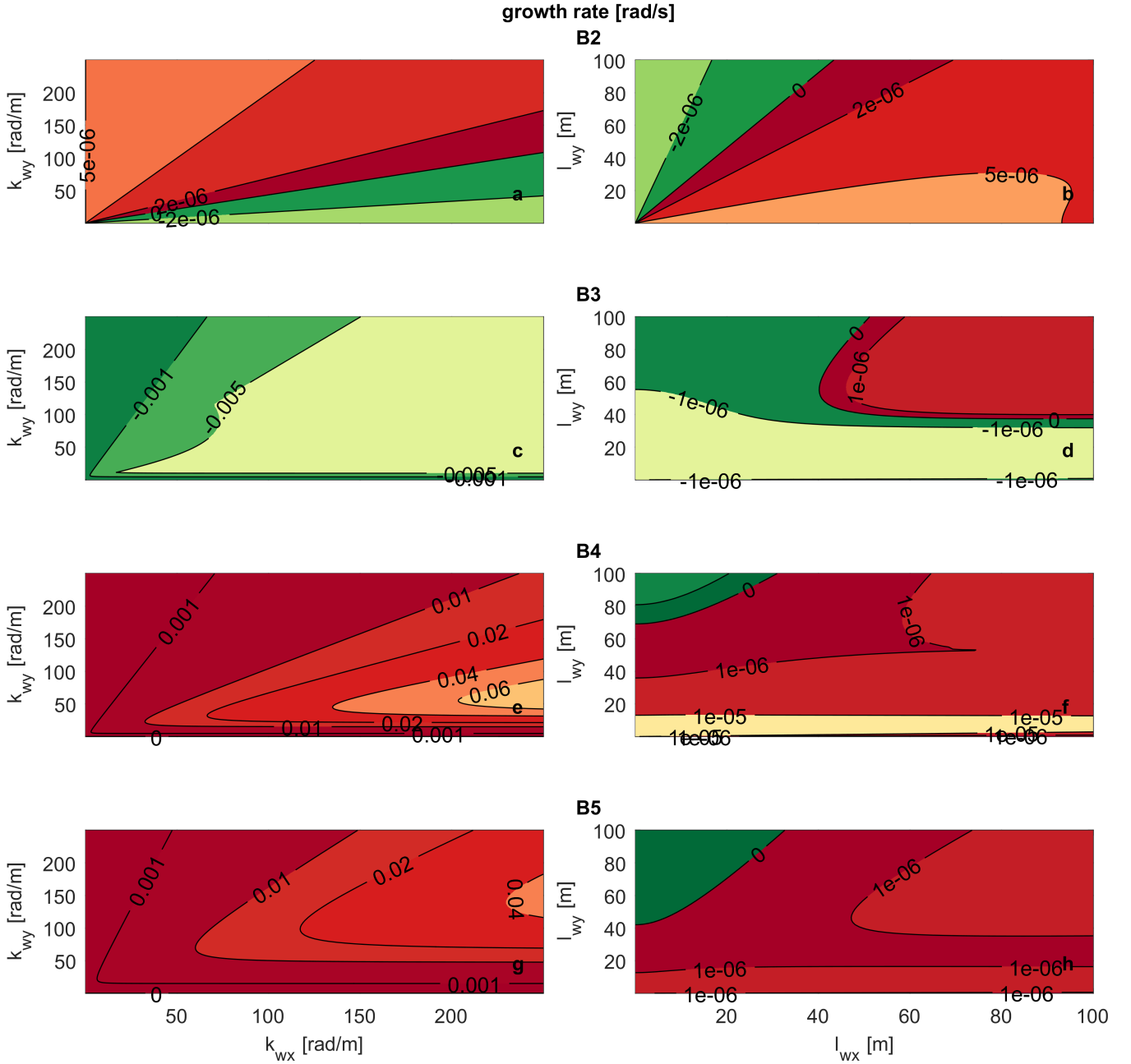
Figure 5: Growth rate of perturbations added to the reference case (tables 1 and 5) as a function of the wave number and the wavelength: (**a**)-(**b**) Case B2 (ill-posed), (**c**)-(**d**) Case B3 (well-posed), (**e**)-(**f**) Case B4 (ill-posed), and (**g**)-(**h**) Case B5 (ill-posed). The subplots in the two columns show the same information but highlight the behaviour for large wave numbers (left column) and for large wavelengths (right column). Red and green indicates growth and decay of perturbations, respectively.

528 r_{y1} is too small (i.e., the bed slope effect is not sufficiently strong) perturbations in the transverse

529 direction are not dampened and the model is ill-posed. On the other hand, for a given r_{y1}, if

530 parameter $d_{x1,1}$ is too small (e.g. due to relatively strong hiding or in conditions close to incipient

531 motion) perturbations in the streamwise direction do not decay and the model is also ill-posed.

532 The critical values $r_{y1}^{\pm}$ that allow for a well-posed model are shown in Appendix E.

533   In Cases B3-B5 we illustrate the possibility of ill-posedness due to the bed slope closure relation

534   (table 5). In Case B3 the sediment mixture consists of two grain size fractions with characteristic

535   grain sizes equal to $0.001\,\text{m}$ and $0.004\,\text{m}$. The volume fraction content of the fine sediment in the

536   active layer and at the interface between the active layer and the substrate is equal to 0.5. The

537   sediment transport rate is computed using the relation developed by *Ashida and Michiue* (1971).

538   The other parameters are equal to the reference case (table 1). The system is well-posed when

539   the effect of the bed slope does not depend on the bed shear stress (figure 5c). The situation is

540   ill-posed if the effect of the bed slope depends on the bed shear stress (Case B4, table 5, figure 5e).

541   The cause of ill-posedness is not found in the closure relation for the bed slope effect only but in

542   the combination of the closure relation with the flow and bed surface conditions. A case equal to

543   B3 except for the fact that the coarse grain size is equal to $0.012\,\text{m}$ is ill-posed (Case B5, table 5,

544   figure 5g).

545   We assess how the domain of ill-posedness due to the bed slope effect depends on the model

546   parameters. For given sediment sizes, flow, and bed surface texture, parameter B_s (equation (23))

547   controls the effect of the bed slope by modifying r_{y1} only. The parameter A_s (equation (23)) cancels

548   in r_{y1} and does not play a role. For this reason we study how $g_{s1}/A_s\ [-]$ affects the domain of

549   ill-posedness for varying sediment properties, flow, and bed surface grain size distribution (figure

550   6). We consider Case B3 and we vary B_s between 0 and 0.5 to vary the bed slope effect. The

551   sediment size of the coarse fraction varies between d_1 and $0.020\,\text{m}$. The mean flow velocity varies

552   between $1\,\text{m/s}$ and $2.8\,\text{m/s}$. The volume fraction content of fine sediment at the bed surface varies

553   between 0 and 1. We aim to isolate the problem of ill-posedness due to bed slope effect from the

554   problem of ill-posedness due to a different grain size distribution at the bed surface and at the

555   interface between the bed surface and the substrate (*Chavarrías et al.*, 2018). For this reason, in

556   this analysis the volume fraction content of fine sediment at the interface is equal to the one at the

557   bed surface. Under this condition the problem can be ill-posed due to the effect of the bed slope

558   only.

559   As we have shown analytically, under unisize conditions (i.e., $d_1/d_2 = 1$ or $F_{a1} = 1$ or $F_{a1} = 0$)

560   the model is well-posed (figure 6a and 6c). For sufficiently different grain sizes ($d_1/d_2 \lessgtr 0.15$)

561   the model is well-posed regardless of the bed slope effect but for a small range of values ($0.08 \lessgtr$

562    $d_1/d_2 \lessgtr 0.1$). This small range of ill-posed values is associated with r_{y1} increasing for decreasing

563   values of d_1/d_2 and acquiring a value larger than r_{y1}^+ such that the model becomes ill-posed for all

564   values of the bed slope effect. A further decrease in d_1/d_2 increases the limit value r_{y1}^+ faster than

565   r_{y1} such that the model becomes well-posed for all values of the bed slope effect.

566   An increase in the Froude number decreases the domain of well-posedness, which is explained

567   from the fact that an increase in Froude number decreases r_{y1} while it does not modify r_{y1}^-. We have

568   assumed steady flow in deriving ω_i^{lim} to reduce the complexity of the model such that we can find

569   an analytical solution (Appendix E). This causes a physically unrealistic resonance phenomenon

570   for $\text{Fr} \to 1$ (*Colombini and Stocchino*, 2005). In reality we do not expect that for Fr=1 the model is
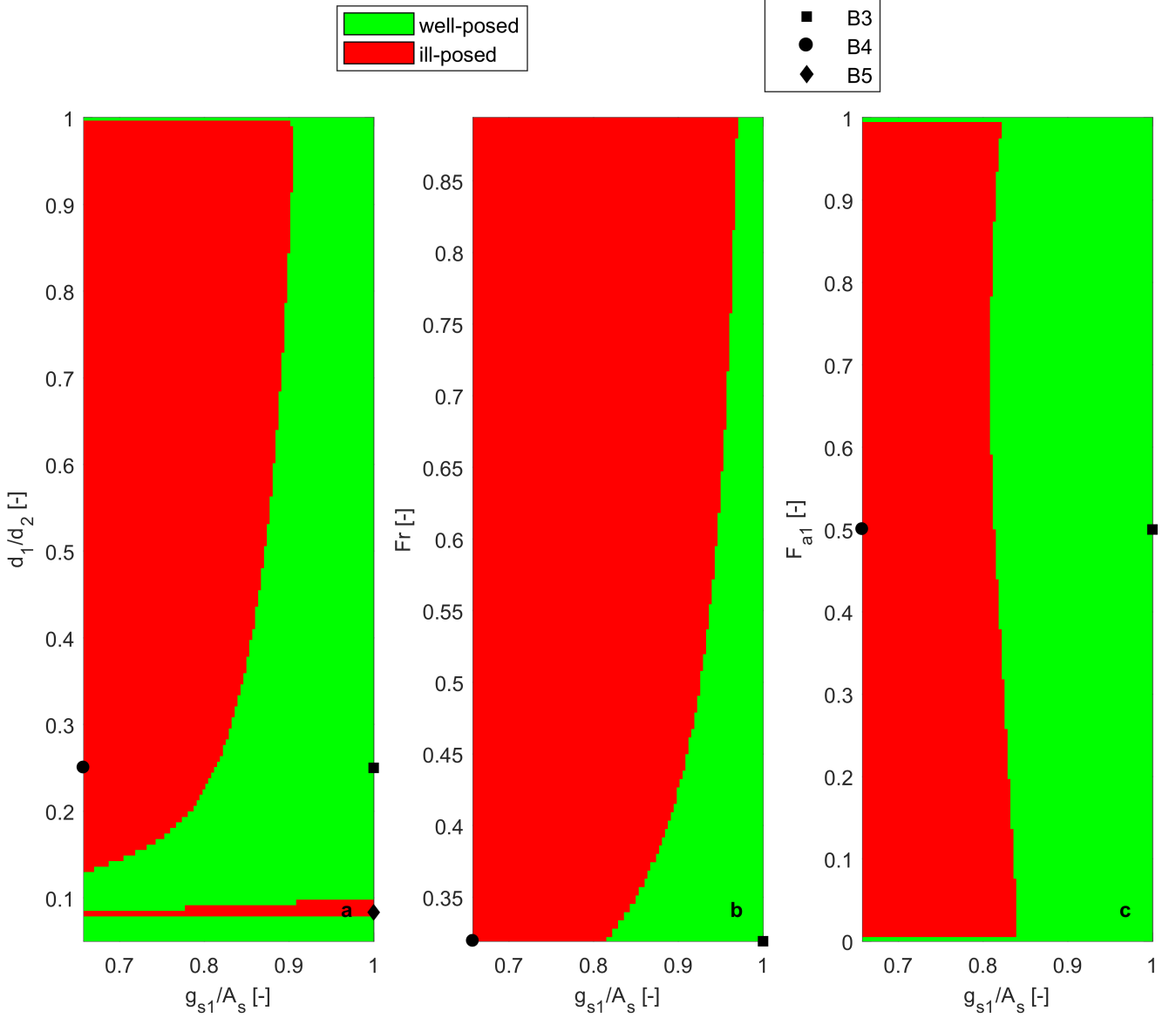
Figure 6: Domain of ill-posedness due to the bed slope effect under mixed-size sediment conditions: as a function of the ratio between fine and coarse sediment (**a**), the Froude number (**b**), and the volume fraction content of fine sediment in the active layer (**c**). The bed slope effect is measured by g_{s1}/A_s and the range of parameters is obtained by varying B_s (equation (23)). The range of values of d_1/d_2 is obtained by varying d_2. The range of values of the Froude number is obtained by varying u. The volume fraction content of fine sediment at the interface between the active layer and the substrate is kept equal to the volume fraction content of fine sediment in the active layer. The conditions represent unisize sediment when $d_1/d_2 = 1$, $F_{a1} = 0$, or $F_{a1} = 1$.

always ill-posed regardless of the bed slope effect. Apart from the limit values in which the problem becomes unisize, the surface volume fraction content does not significantly affect the domain of ill-posedness (figure 6c) as it rescales in more or less a similar way $r_{y1}^{\pm}$ and r_{y1}.

While Case B4 is ill-posed because the effect of the bed slope (r_{y1}) is small, Case B5 is ill-posed because parameter $d_{x1,1}$ is small. The different origin of ill-posedness does not cause a significant difference in the growth rate of perturbations as a function of the wave number (figure 5e-g). However, we will find out that the pattern resulting from the perturbations depends on the origin

578 of ill-posedness.

5   Application

580 The results of the linear stability analysis (Section 4) neglect second order terms and non-linear

581 interactions. In this section we study the effects of the terms neglected in the linear analysis

582 and the development of perturbations by means of numerical simulations. We use the software

583 package Delft3D (*Lesser et al.*, 2004). This exercise provides information on the consequences of ill-

584 posedness in numerical simulations and clarifies the limitations of the current modelling approach.

585 We study the effect of secondary flow (Section 5.1) and the bed slope effect (Section 5.2).

5.1   Secondary Flow

587 We run 5 numerical simulations with a fixed bed (i.e., only the flow is computed) to study the

588 role of the secondary flow model and the diffusion coefficient on the ill-posedness of the system

589 of equations. The first 3 simulations reproduce the conditions of Cases S1, S2, and S3 (table 4).

590 The domain is rectangular, 100 m long and 10 m wide. We use square cells with size equal to

591 0.1 m. The time step is equal to 0.01 s and we simulate 10 minutes of flow. We set a constant

592 water discharge and the downstream water level remains constant with time. The initial condition

593 represents normal flow for the values in table 1 (i.e., equilibrium conditions).

594   The simulation not accounting for secondary flow does not present growth of perturbations as

595 predicted by the linear analysis and remains stable with time (figure 7a). We observe growth of

596 perturbations when we account for secondary flow with the diffusion coefficient derived by *Elder*

597 (1959) (figure 7b). The results are physically unrealistic as the flow depth presents variations of

598 up to 7 % of the normal flow depth and the length scale of perturbations is smaller than the

599 flow depth. We have not introduced any perturbation in the initial or boundary conditions which

600 implies that perturbations grow from numerical truncation errors. This supports the fact that the

601 simulation is physically unrealistic. The case with a diffusion coefficient equal to 0 is ill-posed and

602 the solution presents unreasonably large oscillations (figure 7c). These numerical results confirm

603 the results of the linear stability analysis.

604   In the fourth simulation we set a diffusion coefficient 100 times larger than the one derived by

605 *Elder* (1959) (figure 7d). Under this condition the linear analysis predicts all short waves to decay

606 (diamond in figure 4). These numerical results confirm the linear theory. The last simulation is

607 equal to Case S2 except for the fact that we use a coarser grid ($\Delta x = \Delta y = 1$ m). In this case the

608 numerical grid is not sufficiently detailed for resolving the perturbations due to secondary flow and

609 the simulation is stable (figure 7e). This last case highlights an important limitation of a physically

610 unrealistic model. Although Case S2 is mathematically well-posed, the solution presents similarities

611 with ill-posed cases in the sense that a refinement of the grid causes non-physical oscillations to
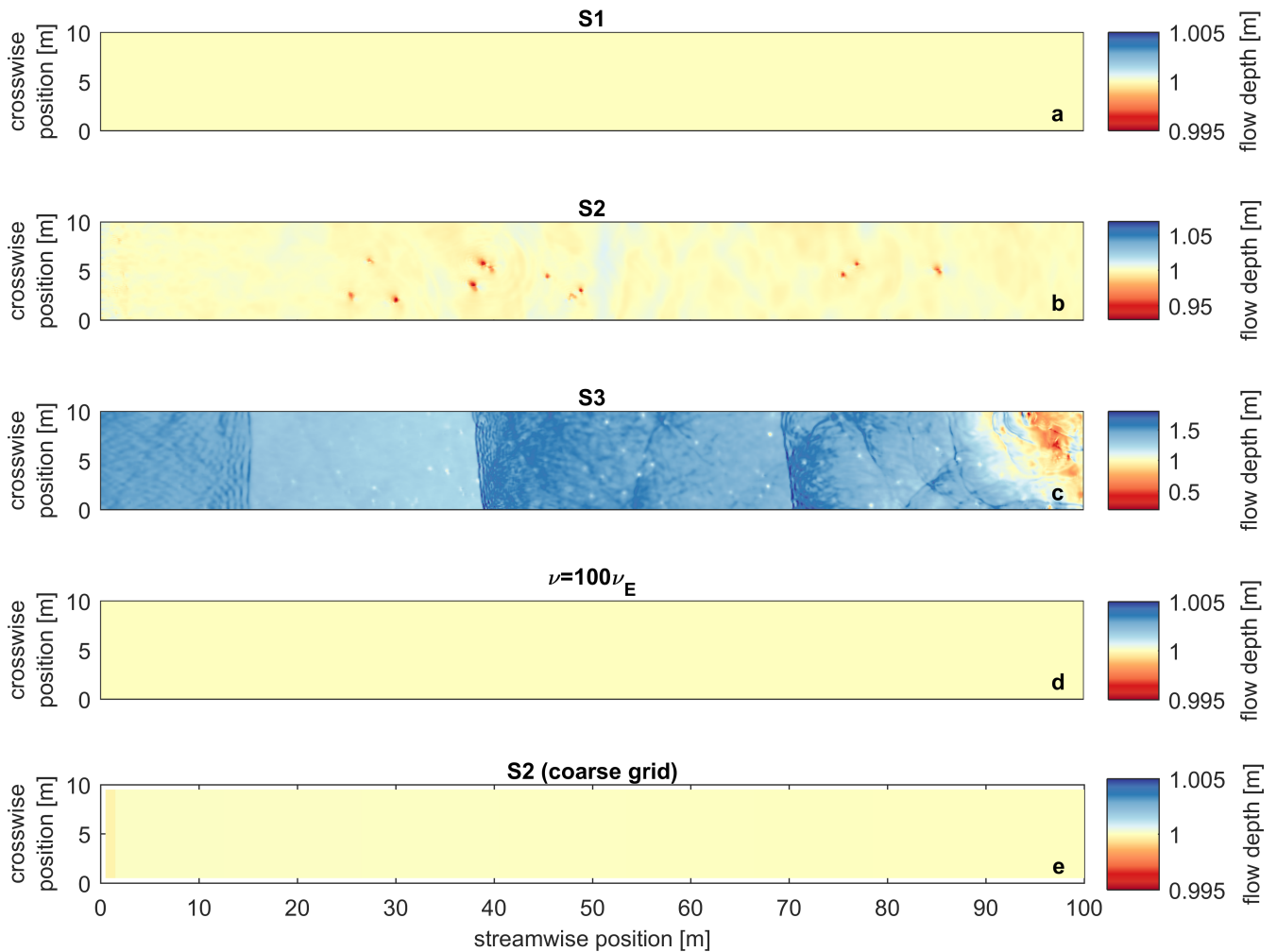
appear.

Figure 7: Flow depth at the end of the simulations: (**a**) without accounting for secondary flow (Case S1), (**b**) setting $\nu = \nu_{\mathrm{E}}$ (Case S2), (**c**) setting $\nu = 0$ (Case S3), (**d**) setting $\nu = 100\nu_{\mathrm{E}}$, and (**e**) setting $\nu = \nu_{\mathrm{E}}$ using a coarser numerical grid (Case S2). The colour map is adjusted for each case and centred around the initial and equilibrium value ($h = 1\,\mathrm{m}$).

5.2   Bed Slope Effect

In this section we focus on the consequences of accounting for the bed slope effect on the mathematical character of the model. To this end we run 5 more numerical simulations without accounting for secondary flow and updating the bed (i.e., accounting for morphodynamic change). The simulations reproduce Cases B1-B5 (table 5). We simulate 8 h using a time step $\Delta t = 0.1\,\mathrm{s}$.

We have proved that accounting for the effect of the bed slope makes a unisize simulation well-posed (Section 4.2 and figure 1c). The numerical solution of this case (B1, table 2) is stable and perturbations do not grow (figure 8a). Moreover, no alternate bars appear as the channel width is below the critical value (Section 3). Perturbations grow when the effect of the bed slope is not taken into account (Case B2, figure 8b), which confirms that this case is ill-posed.

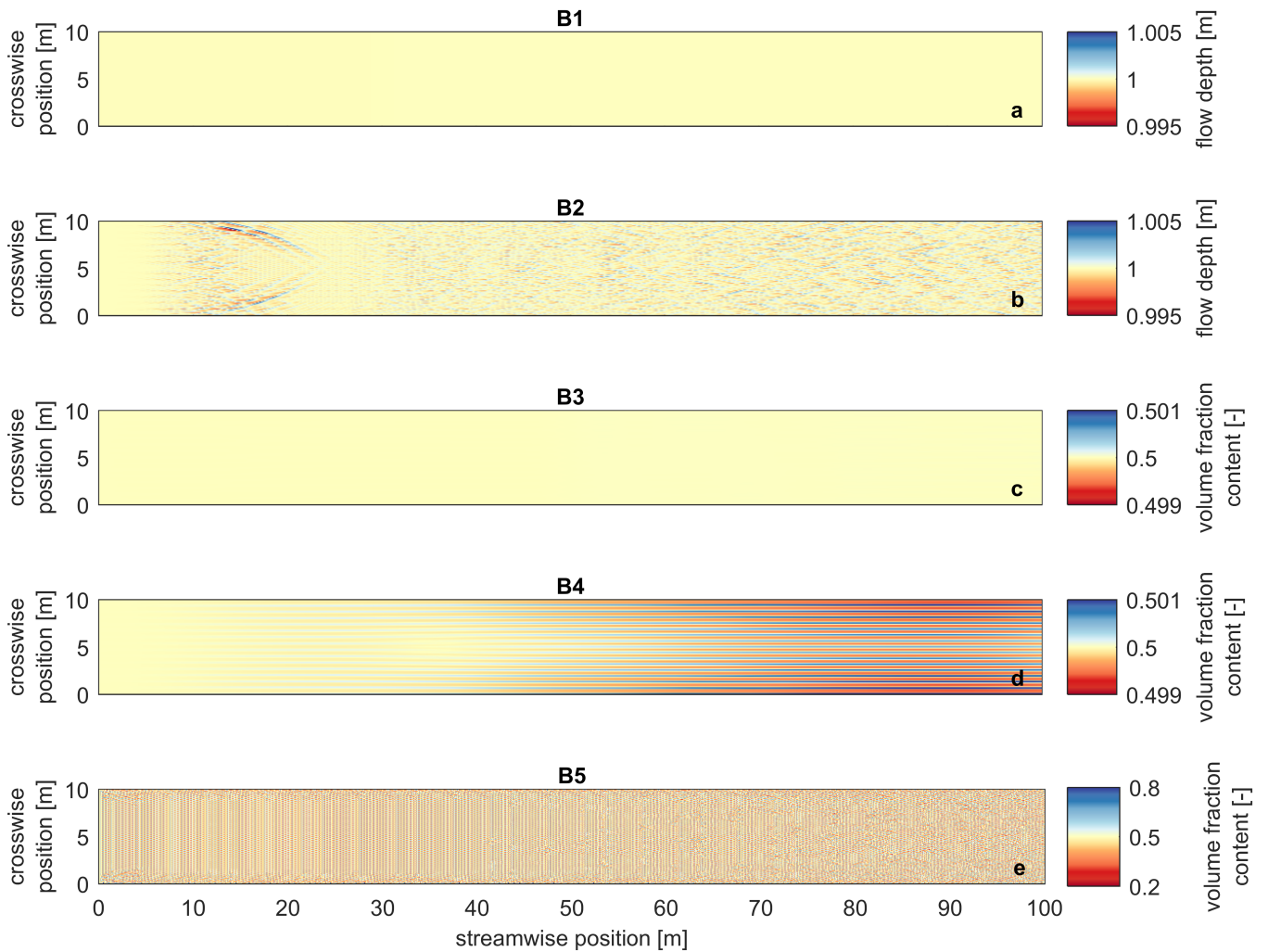The mixed-size sediment conditions of Case B3 yield a well-posed model (figure 5e) and the

Figure 8: Flow depth at the end of the simulations of: (**a**) Case B1, (**b**) Case B2; and volume fraction content of fine sediment in the active layer: (**c**) Case B3, (**d**) Case B4, (**e**) Case B5. The colour map is adjusted for each case and centred around the initial and equilibrium value.

624   simulation is stable (figure 8c). On the other hand, the ill-posed cases B4 and B5 present growth

625   of unrealistic and non-physical perturbations (figure 8d-e). While the growth of perturbations in

626   Case B5 seems random, in Case B4 we observe a clear pattern. Moreover, oscillations have grown

627   significantly faster in Case B5 than in Case B4. While after $8\,\mathrm{h}$ the changes in volume fraction

628   content at the bed surface are of the order of 10^{-3} in Case B4, these are of order 1 in Case B5.

629   The fact that oscillations grow faster in Case B5 than in Case B4 is related to the different origin

630   of ill-posedness. While Case B4 is ill-posed because the effect of the bed slope is not sufficiently

631   strong (i.e., $r_{y1} < r_{y1}^{-}$), Case B5 is ill-posed because changes in the sediment transport rate due

632   to changes in the volume of fine sediment in the active layer are too small (i.e., $r_{y1} > r_{y1}^{+}$). The

633   first case is closely linked to the lateral direction, in which sediment transport is initially zero.

634   The fact that initially the lateral sediment transport rate is zero limits the rate at which lateral

635   changes occur. In the second case perturbations are linked to the streamwise direction, in which

636   the sediment transport rate initially is non-zero, which enhances the rate at which changes develop.

6   Discussion

The origin of the instability due to secondary flow is found in the source term (S_s in equation (11)). As the source term depends on the flow curvature, the source term is 0 in a straight flow. A small perturbation in the flow causes the flow to curve. The flow curvature causes a source of secondary flow intensity, which further increases the flow curvature, causing a positive feedback. The flow curvature is largest for the smallest perturbations, which explains why the model is ill-posed if a dampening mechanism (i.e., diffusion) is not taken into account. This destabilizing mechanism may seem plausible to explain secondary flow circulation observed in straight channels (*Nikuradse*, 1930; *Brundrett and Baines*, 1964; *Nezu and Nakagawa*, 1984; *Gavrilakis*, 1992). However, secondary flow in a straight channel can only be caused by anisotropy of turbulence (*Einstein and Li*, 1958; *Gessner and Jones*, 1965; *Bradshaw*, 1987; *Colombini*, 1993), which is not included in the model for secondary flow. For this reason, the secondary flow model must predict decay of secondary flow intensity in case of straight flow. Diffusion of secondary flow intensity causes decay of perturbations, but the theoretical diffusion coefficient derived by *Elder* (1959) appears to be insufficient to dampen perturbations.

The advection equation of the secondary flow intensity was initially derived for steady decaying secondary flow on a straight reach after a bend neglecting the effect of diffusion (*De Vriend*, 1981). It is assumed that the same advective behaviour is valid for a varying curvature (*De Vriend*, 1981; *Olesen*, 1982) and in an unsteady situation (*Booij and Pennekamp*, 1984). These assumptions have, to our knowledge, not been tested. Moreover, secondary flow affects the vertical profile of the primary flow. This feedback mechanism, which limits the development of secondary flow (*Blanckaert and De Vriend*, 2004; *Blanckaert*, 2009), is not included in the model. *Blanckaert and de Vriend* (2003), *Blanckaert and Graf* (2004) and *Ottevanger et al.* (2013) propose non-linear models that take into consideration this mechanism. We expect that accounting for the feedback mechanism yields a well-posed model.

The feedback mechanism between the secondary and the primary flow may be seen as an increase of diffusivity, as it causes an enhanced momentum redistribution. For a situation in which the non-linear model for the secondary flow appears to be excessively expensive in computational terms, a diffusion coefficient depending on the secondary flow intensity would (partially) account for the enhanced momentum redistribution and provide a well-posed and realistic model.

We have assumed that the diffusion coefficient is constant and equal in all directions, which is a crude approximation, as in the streamwise direction diffusion is larger than in the transverse direction (Appendix A). It would be interesting to study the effect of anisotropic diffusion, however, we do not expect that this will significantly alter our results. This is because a larger diffusion coefficient in the streamwise direction will not alter the most unstable wavelength in the lateral direction. For this reason the shortest unstable waves remain to be of the order of the flow depth.

673   The non-linear relation between the flow and the sediment transport rate causes the growth of

674   perturbations in bed elevation. Worded differently, a deep flow attracts the flow and vice versa,

675   which enhances the growth of perturbations. This mechanism is counteracted by the bed slope

676   effect, which causes deep parts to fill in. In this sense, it seems logical that it is necessary to

677   account for bed slope effects to obtain a well-posed model. This may be confirmed by the facts

678   that *Parker* (1976), by not considering the bed slope effect, found that all streams tend to form

679   bars and, similarly, *Olesen* (1982) concluded that "the stream will develop an infinite number

680   of submerged bars". From our point of view the fact that all streams seem to be unstable and

681   develop an infinite number of submerged bars is a consequence of the model being ill-posed. Our

682   analysis shows that the bed slope effect is a crucial physical process in analysing two-dimensional

683   morphodynamic processes.

684   Nevertheless, the numerical simulations by *Qian et al.* (2016) of bar development without ac-

685   counting for the bed slope effect do not show unrealistic oscillatory behaviour as is characteristic

686   of ill-posedness. Yet, there is an essential difference between their model and the one we analyse

687   here. We do not model the interaction between the sediment in the bed and the sediment in

688   transport as we assume that the sediment transport rate adapts instantaneously to changes in the

689   flow (i.e., the sediment transport rate depends on the flow variables only). Essentially, sediment

690   in transport is not conserved and bed elevation and surface texture changes depend on the diver-

691   gence of the sediment transport rate at capacity conditions. *Qian et al.* (2016) account for the

692   conservation of mass of the sediment in transport and use an entrainment-deposition formulation

693   for modelling bed elevation and surface texture changes (*Parker et al.*, 2000). In this formulation

694   changes depend on the difference between the rate at which sediment is entrained from the bed

695   and at which it is deposited on the bed. The fact that their model does not show symptoms of

696   ill-posedness, while the effect of the bed slope is not taken into consideration, raises the question

697   whether the entrainment-deposition formulation in combination with mass conservation of the sed-

698   iment in transport is responsible, like the bed slope effect, for a mechanism that counteracts growth

699   of perturbations in bed elevation. If the model used by *Qian et al.* (2016) is indeed well-posed,

700   the effect of the bed slope may be a crucial process only when mass conservation of the sediment

701   in transport is not considered.

702   *Lanzoni and Tubino* (1999) investigated the development of alternate bars under mixed-size

703   sediment conditions using a model similar to the one we apply here. They assumed secondary

704   flow to be negligible and considered a different set of closure relations for friction, the sediment

705   transport rate, and the effect of the bed slope. Under the conditions they studied, they found

706   that, similarly to the unisize case, growth of perturbations occurs if the width-to-depth ratio is

707   above a critical value. This implies that they found that their model is well-posed, as short wave

708   length perturbations decay. Given that the essence of the closure relations they considered is the

709   same as the ones considered here and there is no fundamental difference, we suppose that their

710 model may become ill-posed if different conditions are studied (i.e., different flow or sediment

711 parameters). This is because well-posedness is not related to the model equations only, but also

712 to the conditions in which the model is applied.

713 The bed slope effect (represented by the parameter r_{y1}) needs to be balanced with respect

714 to the effect of changes in the bed surface grain size distribution (represented by $d_{x1,1}$) to yield

715 a well-posed model. The balance depends on the flow and bed conditions. For this reason, a

716 particular closure relation may yield an ill-posed model in some subdomain of a simulation and a

717 well-posed model in some other subdomain. It is necessary to further study the development of

718 the transverse bed slope under mixed-size sediment conditions (e.g. *Baar et al.*, 2018) to obtain a

719 universally applicable closure relation.

720 Overall, there are three causes of ill-posedness of the model: (1) the secondary flow parametri-

721 sation, (2) the closure relation for the bed slope effect, and (3) the representation of the vertical

722 mixing processes when using the active layer model (*Ribberink*, 1987; *Chavarrías et al.*, 2018). We

723 summarise all the conditions in which the model may become ill-posed in figure 9.

724 Only in idealised simulations it is straightforward to relate instability of the system of equations

725 to ill-posedness. We advocate for an *a priori* test of whether the system of equations is well-posed

726 or ill-posed, especially when dealing with mixed-size sediment cases. If at some time a location

727 in the model becomes ill-posed, the model results should be carefully evaluated. The fact that

728 some domain area has always been well-posed does not guarantee a unique solution, as oscillations

729 caused by upstream or downstream ill-posed areas propagate through the domain. Similarly, the

730 fact that the entire domain is well-posed at some time is no guarantee of a unique solution, as past

731 oscillations due to ill-posedness affect the present solution.
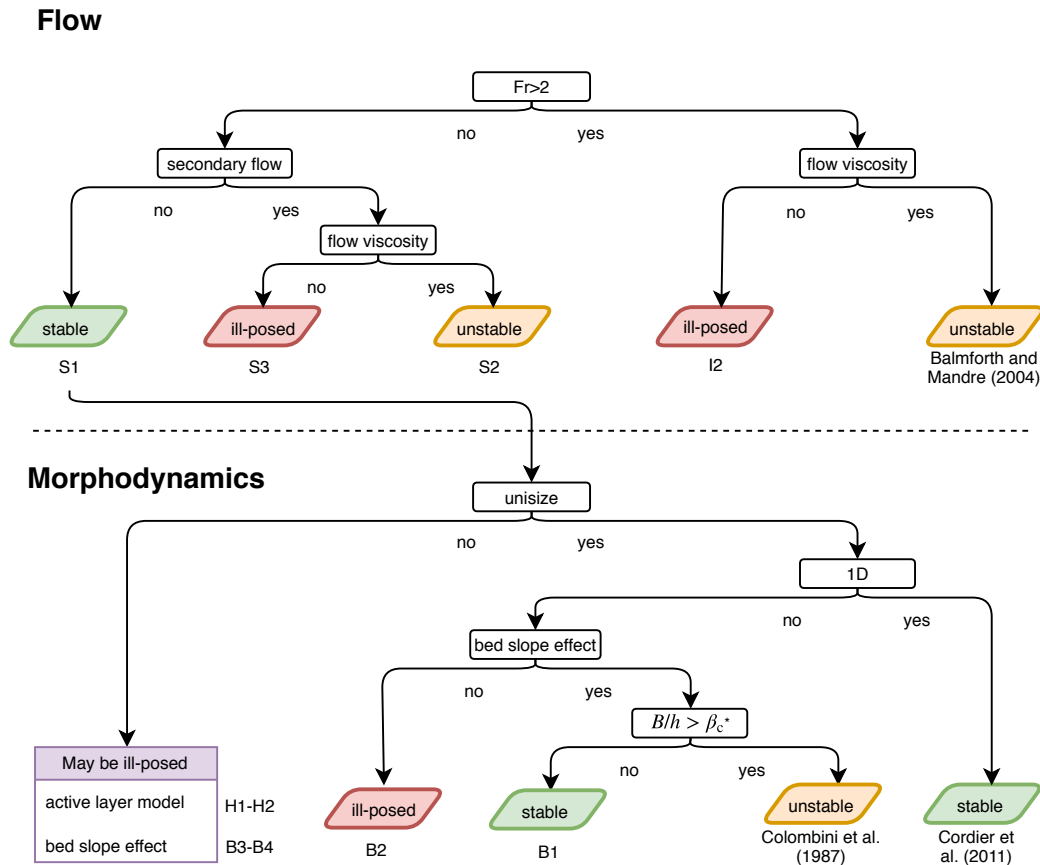
Flow

Figure 9: Conditions in which the flow model (top) and the morphodynamic model (bottom) is stable, unstable, or ill-posed. The code below the model type (e.g., S1) indicates an example case of such a situation. See tables 2, 3, 4, and 5 for an explanation of the cases S1-3, B1-4, H1-2, and I2. * Parameter β_c denotes the critical width-to-depth ratio (*Engelund and Skovgaard*, 1973; *Colombini et al.*, 1987; *Schielen et al.*, 1993).

7   Conclusions

We have studied a two-dimensional system of equations used to model mixed-size river morphodynamics as regards to its well-posedness. The model is based on the depth-averaged Shallow Water Equations in combination with the *Exner* (1920) and active layer (*Hirano*, 1971) equations to model bed elevation and surface texture changes, respectively. In particular we have focused on modelling of the secondary flow induced by flow curvature and the effect of the bed slope on the sediment transport direction, which causes particles to deviate from the direction of the bed shear stress.

By means of a linear stability analysis of the system of equations we find that:

- The parametrisation accounting for secondary flow yields an ill-posed model if diffusion is not accounted for.

- The theoretical amount of diffusion due to depth-averaging the vertical profile of the primary flow (*Elder*, 1959) yields a well-posed model but it predicts growth of perturbations that are incompatible with the shallow water assumption.

- The effect of the bed slope on the direction of the sediment transport is a necessary mechanism for the model being well-posed. Yet, a different modelling strategy accounting for conservation of the sediment in transport and an entrainment-deposition formulation may yield a well-posed model without accounting for the effect of the bed slope.

- Not all closure relations accounting for the bed slope effect are valid under mixed-size sediment conditions. There needs to be a balance between the effect of the bed slope and the effect of the streamwise variation of grain size distribution on the sediment transport rate.

Numerical simulations of idealised cases confirm the above results of the linear stability analysis.

Acknowledgements

A   Eddy Viscosity

In general terms, given the anisotropy of the flow field, the diffusion tensor has non-diagonal terms and the diagonal terms are not equal (i.e., the diffusion coefficient in the streamwise direction ν_s is different than in the transverse direction ν_n). The non-diagonal terms become significant close to corners (*Fischer*, 1973) but far from corners the diagonal terms dominate. *Elder* (1959) derived an eddy viscosity coefficient in the streamwise and lateral direction assuming a logarithmic profile for the primary flow:

$$\nu_\mathrm{s} = \left(\frac{0.4041}{\kappa^3} + \frac{1}{6}\kappa \right) h u^* \,, \tag{37}$$

$$\nu_\mathrm{n} = \frac{1}{6}\kappa h u^* \,. \tag{38}$$

Elder neglected the effect of the viscous sublayer, which causes his analytical expression to be a lower limit of the diffusion coefficient (*Fischer*, 1967).

Several researchers (e.g. *Erdogan and Chatwin*, 1967; *Simons and Albertson*, 1963; *Fischer*, 1969; *Holley*, 1971; *Fischer*, 1973; *Kyong and Il*, 2016) propose values for the diffusion coefficient that are significantly larger than the one derived by *Elder* (1959). These values are used, for instance, by *Parker* (1978); *Ikeda and Nishimura* (1985) and *Van Prooijen and Uijttewaal* (2002). These values of the diffusion coefficient are derived from experimental measurements and implicitly account for the enhanced momentum redistribution due to secondary flow that we account for by means of the dispersive stresses.

778   In numerical simulations resolving the secondary flow, the diffusion coefficients derived by *Elder*

779   (1959) are valid if the grid is of the order of magnitude of the flow depth (assuming that the relevant

780   turbulent processes scale with the flow depth). Otherwise the numerical grid filters out significant

781   two-dimensional turbulent motions that need to be accounted for in the closure model (*Talstra*,

782   2011). In our numerical runs the grid cell size is always smaller than the flow depth.

B   Magnitude of the Sediment Transport Rate

784   The module of the specific sediment transport rate of size fraction k, q_{bk} [m^2/s], has a direction

785   given by the angle φ_{sk} [rad]:

$$(q_{bxk}, q_{byk}) = q_{bk}(\cos \varphi_{sk}, \sin \varphi_{sk}) . \tag{39}$$

787   The magnitude of the sediment transport rate is equal to:

$$q_{bk} = F_{ak}\sqrt{gRd_k^3}\,(1 - p)\,q_{bk}^* , \tag{40}$$

789   where p is the porosity and q_{bk}^* [−] is a nondimensional sediment transport rate (*Einstein*, 1950)

790   dependent on the *Shields* (1936) stress:

$$\theta_k = \frac{C_f \left(\frac{Q}{h}\right)^2}{gRd_k} . \tag{41}$$

792   The parameter $R = \rho_s/\rho_w - 1$ [−] is the submerged sediment density, $\rho_s = 2650\,\text{kg/m}^3$ is the

793   sediment density and $\rho_w = 1000\,\text{kg/m}^3$ is the water density. To compute the nondimensional

794   sediment transport rate we use a fractional form (*Blom et al.*, 2016, 2017) of the relation proposed

795   by *Engelund and Hansen* (1967) neglecting form drag:

$$q_{bk}^* = \frac{0.05}{C_f}\theta_k^{5/2} , \tag{42}$$

797   and the relation including a nondimensional critical shear stress θ_c [−] proposed by *Ashida and*

798   *Michiue* (1971):

$$q_{bk}^* = 17\,(\theta_k - \xi_k\theta_c)\left(\sqrt{\theta_k} - \sqrt{\xi_k\theta_c}\right) . \tag{43}$$

800   The parameter ξ_k [−] is the hiding factor that accounts for the fact that fine sediment in a mixture

801   hides behind larger grains and a coarse sediment in a mixture is more exposed than in unisize

802 coarse sediment (*Einstein*, 1950). *Ashida and Michiue* (1971) proposes $\theta_\mathrm{c} = 0.05$ and the relation:

803
$$\xi_k = \begin{cases} 0.843 \left(\frac{d_k}{D_\mathrm{m}} \right)^{-1} & \text{for } \frac{d_k}{D_\mathrm{m}} \leq 0.4 \\ \left(\frac{\log_{10}(19)}{\log_{10}(19 \frac{d_k}{D_\mathrm{m}})} \right)^2 & \text{for } \frac{d_k}{D_\mathrm{m}} > 0.4 \end{cases} , \tag{44}$$

804 where D_m is a characteristic mean grain size of the sediment mixture.

C Proof of Ill-posedness Due to Secondary Flow without Diffusion

807 In this section we prove that the model based on the Shallow Water Equations accounting for
808 secondary flow without diffusion is ill-posed.

809   The system of equations is composed of the first four rows and columns of the full system of
810 equations in equation (24). Neglecting diffusive processes matrices $\mathbf{D_{x0}}$ and $\mathbf{D_{y0}}$ are equal to $\mathbb{0}$.
811 As we are interested in the short-wave domain, friction can be neglected. The resulting matrix
812 $\mathbf{M_0}$ of the linearised eigenvalue problem (equation (33)) is:

813
$$\mathbf{M_0} = \mathbf{A_{x0}} k_\mathrm{wx} + \mathbf{A_{y0}} k_\mathrm{wy} . \tag{45}$$

814   We compute the fourth order characteristic polynomial of matrix $\mathbf{M_0}$. The roots of the char-
815 acteristic polynomial are the eigenvalues (i.e., the angular frequencies ω in equation (31)). The
816 discriminant of a fourth order polynomial $p(\omega) = p_4\omega^4 + p_3\omega^3 + p_2\omega^2 + p_1\omega + p_0 = 0$ is equal to
817 (*Beeler et al.*, 1972):

818
$$\begin{aligned} \Delta_4 = & (p_1^2 p_2^2 p_3^2 - 4p_1^3 p_3^3 - 4p_1^2 p_2^3 p_4 + 18p_1^3 p_2 p_3 p_4 - 27p_1^4 p_4^2 + 256p_0^3 p_4^3) \\ & + p_0(-4p_2^3 p_3^2 + 18p_1 p_2 p_3^3 + 16p_2^4 p_4 - 80p_1 p_2^2 p_3 p_4 - 6p_1^2 p_3^2 p_4 + 144p_1^2 p_2 p_4^2) \\ & + p_0^2(-27p_3^4 + 144p_2 p_3^2 p_4 - 128p_2^2 p_4^2 - 192p_1 p_3 p_4^2) . \end{aligned} \tag{46}$$

819 We find that the discriminant of the characteristic polynomial is:

820
$$\Delta_4 = \frac{16gh^2 T^2 \beta_\mathrm{u}}{L_\mathrm{I}} k_\mathrm{wx}^2 \left(k_\mathrm{wx}^2 - k_\mathrm{wy}^2 \right) , \tag{47}$$

821 where $\beta_\mathrm{u} = \beta^* q_\mathrm{x}^2 / h^2$ and:

822
$$T = L_\mathrm{I} g \left[L_\mathrm{I} g \left(k_\mathrm{wx}^2 + k_\mathrm{wy}^2 \right)^2 + \beta_\mathrm{u} \left(6k_\mathrm{wx}^2 k_\mathrm{wy}^2 - 2k_\mathrm{wx}^4 \right) \right] + \beta_\mathrm{u}^2 k_\mathrm{wx}^4 . \tag{48}$$

823 As the coefficients of the characteristic polynomial $p(\omega)$ are all real, a positive discriminant indicates
824 that either all the roots are real or all the roots are complex. A negative discriminant indicates that

there are two real and two complex roots. The complex roots come in pairs of complex conjugates. For this reason, if the discriminant is negative there exist an eigenvalue with a positive imaginary component. As the discriminant is negative for $k_{wx} < k_{wy}$ independently from the wave number, there exists always a region of growth. This implies that the model is ill-posed.

D Proof of Ill-posedness Due to Lack of Bed Slope Effect under Unisize Conditions

In this section we prove that the model based on the Shallow Water Equations without accounting for the effect of secondary flow in combination with the *Exner* (1920) equation to model bed elevation changes is ill-posed if the effect of the bed slope on the direction of the sediment transport is not taken into consideration.

The system of equations is composed of the first three and the fifth rows and columns of the system of equations in equation (24). Neglecting diffusive processes in the momentum equations and the effect of the bed slope, matrices $\mathbf{D_{x0}}$ and $\mathbf{D_{y0}}$ are equal to $\mathbb{0}$. The system of equations has 4 unknowns (h, q_x, q_y, and η). The unknowns are coupled meaning that a change in bed elevation influences the flow and vice versa. The celerity of perturbations associated with the flow variables (i.e., h, q_x, and q_y) are orders of magnitude larger than the celerity of perturbations in bed elevation if the Froude number is sufficiently small (Fr $\lessapprox$ 0.7 (*De Vries*, 1965, 1973; *Lyn and Altinakar*, 2002)). Under this condition we can decouple the system and consider steady flow to study the propagation of perturbations in bed elevation (i.e., quasi-steady flow assumption (*De Vries*, 1965; *Cao and Carling*, 2002; *Colombini and Stocchino*, 2005)). In this manner we reduce the number of unknowns to one (η), which means that there is only one eigenvalue (ω). We obtain ω equating to 0 the determinant of matrix:

$$\mathbf{R} = \begin{bmatrix} 0 & 0 & 0 & 0 \\ 0 & 0 & 0 & 0 \\ 0 & 0 & 0 & 0 \\ 0 & 0 & 0 & \omega \end{bmatrix} - \mathbf{M_0} \quad . \tag{49}$$

The growth rate (the imaginary part of ω) is:

$$\omega_i = \frac{q_b C_f k_{wx}^2}{k_{wx}^2 w_2^2 + w_1^2} \left(w_3 + (n-1) k_{wy}^4 \right) \ , \tag{50}$$

where w_1, w_2, and w_3 are second degree polynomials on k_{wy}:

$$w_1 = C_f \left[\left(1 - 4\mathrm{Fr}^2\right) k_{wx}^2 + 2k_{wy}^2 \right] \ , \tag{51}$$

$$w_2 = b_1 + \left(1 - \mathrm{Fr}^2\right) k_{\mathrm{wx}}^2 + k_{\mathrm{wy}}^2 \ , \tag{52}$$

$$w_3 = -3\mathrm{Fr}^2 n k_{\mathrm{wx}}^4 - b_1 n k_{\mathrm{wx}}^2 + \left[n \left(2 - \mathrm{Fr}^2\right) - \left(2 + \mathrm{Fr}^2\right)\right] k_{\mathrm{wx}}^2 k_{\mathrm{wy}}^2 + b_1 \left(n - 3\right) k_{\mathrm{wy}}^2 \ , \tag{53}$$

where b_1 is:

$$b_1 = \frac{3 C_{\mathrm{f}}^2 \mathrm{Fr}^2}{h^2} \ . \tag{54}$$

Parameter n is the degree of non-linearity of the sediment transport relation (*Mosselman et al.*, 2008):

$$n = \frac{Q}{q_{\mathrm{b}}} \frac{\partial q_{\mathrm{b}}}{\partial Q} \ , \tag{55}$$

which is larger than 1. For instance, $n = 5$ in the relation developed by *Engelund and Hansen* (1967) and $n > 3$ in the one by *Meyer-Peter and Müller* (1948). In general $n > 3$ for the sediment transport relation to be physically realistic (*Mosselman*, 2005).

For k_{wy} tending to infinity, parameter w_3 becomes negligible with respect to $(n - 1)k_{\mathrm{wy}}^4$. As all other terms in equation (50) are positive, for a large wave number the growth rate is positive which implies that the model is ill-posed.

E Well-Posed Domain under Mixed-Size Sediment Conditions

In this section we show that the Shallow Water Equations in combination with the active layer model (*Hirano*, 1971) used to account for mixed-size sediment morphodynamics may yield an ill-posed model depending on the closure relation used to account for the effect of the bed slope on the sediment transport direction.

We consider a model with two sediment size fractions. The system of equations is composed of the first three, the fifth and the sixth rows and columns of the full system of equations in equation (24). We neglect diffusive processes in the momentum equations. The system of equations has 5 unknowns (h, q_{x}, q_{y}, η, and M_{a1}). We consider that the Froude number is sufficiently small such that the quasi-steady approximation is valid (Appendix D) and we assume that the celerity associated with changes in the grain size distribution of the bed surface are of the same order of magnitude as the celerity of bed elevation changes (*Ribberink*, 1987; *Sieben*, 1997; *Stecca et al.*, 2016). Under these conditions it is valid to decouple the system and consider steady flow to study the propagation of perturbations in bed elevation and bed surface grain size distribution. In this manner we reduce the number of unknowns to two (η and M_{a1}), which means that there are two

882 angular frequencies to find. We obtain ω equating to 0 the determinant of matrix:

$$
\mathbf{R} = \begin{bmatrix} 0 & 0 & 0 & 0 & 0 \\ 0 & 0 & 0 & 0 & 0 \\ 0 & 0 & 0 & 0 & 0 \\ 0 & 0 & 0 & \omega & 0 \\ 0 & 0 & 0 & 0 & \omega \end{bmatrix} - \mathbf{M_0} \qquad .
$$

883   (56)

884   We define a set of physically meaningful parameters useful to simplify the expression of the

885 growth rate. Subscripts k and l refer to the grain size fraction while the subscript j refers to the

886 direction (i.e., x and y). The parameters are a generalization of the parameters used by *Stecca*

887 *et al.* (2014) and *Chavarrías et al.* (2018) to the x and y direction.

888   Parameter ψ_j [$-$] represents the sediment transport intensity (e.g. *De Vries*, 1965; *Lyn and*

889 *Altinakar*, 2002; *Stecca et al.*, 2014) and ranges between 0 (no sediment transport) and $\mathcal{O}(10^{-2})$

890 (high sediment discharge):

891
$$
\psi_j = \frac{\partial q_{\mathrm{b}j}}{\partial q_j} \quad . \tag{57}
$$

892 Parameter $c_{jk} \in [0,1]$ [$-$] represents the sediment transport intensity of fraction k relative to the

893 total sediment transport intensity:

894
$$
c_{jk} = \frac{1}{\psi_j} \frac{\partial q_{\mathrm{b}jk}}{\partial q_j} \quad . \tag{58}
$$

895 Parameter γ_{jk} [$-$] represents the sediment transport intensity of fraction k relative to the fraction

896 content of sediment of fraction k at the interface between the active layer and the substrate:

897
$$
\gamma_{jk} = c_{jk} - f_k^{\mathrm{I}} \quad , \tag{59}
$$

898 Parameter χ_{jk} [$-$] represents the nondimensional rate of change of the total sediment transport

899 rate with respect to the change of volume of sediment of size fraction k in the active layer:

900
$$
\chi_{jk} = \frac{1}{u_j} \frac{\partial q_{\mathrm{b}j}}{\partial M_{\mathrm{a}k}} \quad . \tag{60}
$$

901 Parameter $d_{jk,l}$ [$-$] represents the nondimensional rate of change of the sediment transport rate of

902 size fraction l with respect to the volume of sediment of size fraction k in the active layer:

903
$$
d_{jk,l} = \frac{1}{u_j \chi_{jk}} \frac{\partial q_{\mathrm{b}jl}}{\partial M_{\mathrm{a}k}} \quad . \tag{61}
$$

904 Parameter $\mu_{jk,l}$ [$-$] represents the rate of change of the sediment transport rate with respect to

905 the volume of sediment in the active layer relative to the fraction content of sediment of fraction

k at the interface between the active layer and the substrate:

$$\mu_{jk,l} = d_{jk,l} - f_k^{\mathrm{I}} \;.$$

(62)

Parameter $R_j < 0 \; [\mathrm{m^2/s}]$ represents the effect of the bed slope on the direction of the sediment transport rate:

$$R_j = \frac{\partial q_{\mathrm{b}j}}{\partial s_j} \;,$$

(63)

where $s_j = \partial\eta/\partial j$. Parameter $r_{jk} \; [-]$ represents the effect of the bed slope on the direction of the sediment transport rate of fraction k relative to the total effect:

$$r_{jk} = \frac{1}{R_j} \frac{\partial q_{\mathrm{b}jk}}{\partial s_j} \;.$$

(64)

Parameter $l_{jk} \; [-]$ represents the effect of the bed slope on the direction of the sediment transport rate of fraction k relative to the fraction content of sediment at the interface between the active layer and the substrate:

$$l_{jk} = r_{jk} - f_k^{\mathrm{I}} \;.$$

(65)

The largest of the two growth rates (i.e., the largest imaginary part of the two eigenvalues ω of the system) is:

$$\omega_{\mathrm{i}} = \frac{1}{2} \left(\frac{\sqrt{2}}{2} \sqrt{f_1} - \sqrt{f_2} \right) \;,$$

(66)

where:

$$f_1 = \sqrt{m_1^2 + m_2} - m_1 \;,$$

(67)

and:

$$f_2 = R_{\mathrm{y}}^2 k_{\mathrm{wy}}^4 \;.$$

(68)

When parameter f_1 is larger than $2f_2$, $\omega_{\mathrm{i}} > 0$ and perturbations grow. Parameter f_1 becomes large with respect to f_2 when parameter m_2 becomes large with respect to m_1 where:

$$m_1 = k_{\mathrm{wx}}^2 u^2 a_3 - f_2 \;,$$

(69)

and:

$$m_2 = 4 k_{\mathrm{wx}}^2 u^2 f_2 o^2 \;.$$

(70)

Focusing on the bed slope effect, for a given value of f_2 (i.e., a given value of R_{y}), parameter m_2 becomes large with respect to m_1 when parameter o becomes large, where:

$$o = a_1 + 2\chi_{\mathrm{x}1} \left(r_{\mathrm{y}1} - d_{\mathrm{x}1,1} \right) \;.$$

(71)

Thus, the growth rate of perturbations is prone to be positive when the absolute value of $r_{y1} - d_{x1,1}$ increases. The parameters a_m for $m = 1, 2, 3$ are:

$$a_1 = e_x + e_y + \chi_{x1}\mu_{x1,1} \, , \tag{72}$$

$$a_2 = \gamma_{x1}e_x + \gamma_{y1}e_y - \mu_{x1,1}e_x - \mu_{x1,1}e_y \, , \tag{73}$$

$$a_3 = a_1^2 + 4\chi_{x1}a_2 \, . \tag{74}$$

The parameters e_j for $j = x, y$ are:

$$e_x = \psi_x \frac{k_{wx}^2}{\left(1 - \mathrm{Fr}^2\right) k_{wx}^2 + k_{wy}^2} \, , \tag{75}$$

$$e_y = \psi_y \frac{k_{wy}^2}{\left(1 - \mathrm{Fr}^2\right) k_{wx}^2 + k_{wy}^2} \, . \tag{76}$$

We compute the limit of the growth rate (equation (66)) for k_{wx} and k_{wy} tending to infinity:

$$\omega_i^{\mathrm{lim}} = \alpha_1 \left(r_{y1} - d_{x1,1}\right)^2 + \alpha_2 \left(r_{y1} - d_{x1,1}\right) + \alpha_3 \, , \tag{77}$$

where:

$$\alpha_1 = \frac{-u^2\chi_{x1}}{R_y}\chi_{x1} \, , \quad \alpha_2 = \frac{-u^2\chi_{x1}}{R_y}a_1^{\mathrm{lim}} \, , \quad \alpha_3 = \frac{u^2\chi_{x1}}{R_y}a_2^{\mathrm{lim}} \, , \tag{78}$$

where the superscript lim indicates that these are the limit values and:

$$e_x^{\mathrm{lim}} = \frac{\psi_x}{2 - \mathrm{Fr}^2} \, , \tag{79}$$

$$e_y^{\mathrm{lim}} = \frac{\psi_y}{2 - \mathrm{Fr}^2} \, . \tag{80}$$

As $R_y < 0$ and $\chi_{x1} > 0$, the mathematical character of the system of equations is given by the sign of the second degree polynomial with variable $(r_{y1} - d_{x1,1})$. The fact that $\alpha_1 > 0$ (the factor of the squared term) indicates that the model is well-posed when $r_{y1}^- < r_{y1} < r_{y1}^+$ where:

$$r_{y1}^{\pm} = \frac{1}{2\chi_{x1}} \left(-a_1^{\mathrm{lim}} \pm \sqrt{a_1^{\mathrm{lim}^2} + 4\chi_{x1}a_2^{\mathrm{lim}}}\right) + d_{x1,1} \, . \tag{81}$$

References

Armanini, A., and G. di Silvio (1988), A one-dimensional model for the transport of a sediment mixture in non-equilibrium conditions, *J. Hydraul. Res.*, *26*(3), 275–292, doi:10.1080/

960   00221688809499212.

961   Ashida, K., and M. Michiue (1971), An investigation of river bed degradation downstream of a

962   dam, in *Proc. of the 14th IAHR World Congress, 29 August–3 Septemeber, Paris, France*, vol. 3,

963   pp. 247–255.

964   Baar, A. W., J. de Smit, W. S. J. Uijttewaal, and M. G. Kleinhans (2018), Sediment transport of

965   fine sand to fine gravel on transverse bed slopes in rotating annular flume experiments, *Water*

966   *Resour. Res.*, *54*, doi:10.1002/2017WR020604.

967   Balmforth, N. J., and S. Mandre (2004), Dynamics of roll waves, *J. Fluid Mech.*, *514*, 1–33, doi:

968   10.1017/S0022112004009930.

969   Balmforth, N. J., and A. Vakil (2012), Cyclic steps and roll waves in shallow water flow over an

970   erodible bed, *J. Fluid Mech.*, *695*, 35–62, doi:10.1017/jfm.2011.555.

971   Banks, J., J. Brooks, G. Cairns, G. Davis, and P. Stacey (1992), On Devaney's definition of chaos,

972   *The American Mathematical Monthly*, *99*(4), 332–334, doi:10.2307/2324899.

973   Barker, B., M. A. Johnson, P. Noble, L. M. Rodrigues, and K. Zumbrun (2017a), Note on the

974   stability of viscous roll waves, *C. R. Mec.*, *345*(2), 125–129, doi:10.1016/j.crme.2016.11.001.

975   Barker, B., M. A. Johnson, P. Noble, L. M. Rodrigues, and K. Zumbrun (2017b), Stability of

976   viscous St. Venant roll waves: From onset to infinite Froude number limit, *J. Nonlinear Sci.*,

977   *27*(1), 285–342, doi:10.1007/s00332-016-9333-6.

978   Barker, T., and J. M. N. T. Gray (2017), Partial regularisation of the incompressible μ-rheology

979   for granular flow, *J. Fluid Mech.*, *828*, 5–32, doi:10.1017/jfm.2017.428.

980   Barker, T., D. G. Schaeffer, P. Bohorquez, and J. M. N. T. Gray (2015), Well-posed and ill-posed

981   behaviour of the μ-rheology for granular flow, *J. Fluid Mech.*, *779*, 794–818, doi:10.1017/jfm.

982   2015.412.

983   Beeler, M., R. W. Gosper, and R. C. Schroeppel (1972), HAKMEM, *MIT AI Memo 239*, Artificial

984   Intelligence Laboratory, Massachusetts Institute of Technology, Cambridge, MA, United States,

985   107 pp.

986   Begnudelli, L., A. Valiani, and B. F. Sanders (2010), A balanced treatment of secondary currents,

987   turbulence and dispersion in a depth-integrated hydrodynamic and bed deformation model for

988   channel bends, *Adv. Water Resour.*, *33*(1), 17–33, doi:10.1016/j.advwatres.2009.10.004.

989   Bell, R. G., and A. J. Sutherland (1983), Nonequilibrium bedload transport by steady flows, *J.*

990   *Hydraul. Eng.*, *109*(3), doi:10.1061/(ASCE)0733-9429(1983)109:3(351).

van Bendegom, L. (1947), Eenige beschouwingen over riviermorphofogie en rivierverbetering, *De Ingenieur*, *59*(4), 1–11, (in Dutch).

Blanckaert, K. (2009), Saturation of curvature-induced secondary flow, energy losses, and turbulence in sharp open-channel bends: Laboratory experiments, analysis, and modeling, *J. Geophys. Res., Earth Surface*, *114*, F03015, doi:10.1029/2008JF001137.

Blanckaert, K., and H. J. de Vriend (2003), Nonlinear modeling of mean flow redistribution in curved open channels, *Water Resour. Res.*, *39*(12), doi:10.1029/2003WR002068.

Blanckaert, K., and W. H. Graf (2004), Momentum transport in sharp open-channel bends, *J. Hydraul. Eng.*, *130*(3), 186–198, doi:10.1061/(ASCE)0733-9429(2004)130:3(186).

Blanckaert, K., and H. J. de Vriend (2004), Secondary flow in sharp open-channel bends, *J. Fluid Mech.*, *498*, 353–380, doi:10.1017/S0022112003006979.

Blom, A. (2008), Different approaches to handling vertical and streamwise sorting in modeling river morphodynamics, *Water Resour. Res.*, *44*(3), W03415, doi:10.1029/2006WR005474.

Blom, A., E. Viparelli, and V. Chavarrías (2016), The graded alluvial river: Profile concavity and downstream fining, *Geophys. Res. Lett.*, *43*, 6285–6293, doi:10.1002/2016GL068898.

Blom, A., L. Arkesteijn, V. Chavarrías, and E. Viparelli (2017), The equilibrium alluvial river under variable flow and its channel-forming discharge, *J. Geophys. Res., Earth Surface*, *122*, doi:10.1002/2017JF004213.

Booij, R., and J. G. S. Pennekamp (1983), Simulation of main flow and secondary flow in a curved open channel, *Tech. Rep. 10-83*, Laboratory of Fluid Mechanics, Faculty of Civil Engineering and Geosciences, Delft University of Technology, Delft, the Netherlands, 62 pp.

Booij, R., and J. G. S. Pennekamp (1984), Measurements of the rate of adjustement of the secondary flow in a curved open channel with varying discharge, *Tech. Rep. 15-84*, Laboratory of Fluid Mechanics, Faculty of Civil Engineering and Geosciences, Delft University of Technology, Delft, the Netherlands, 44 pp.

Bradshaw, P. (1987), Turbulent secondary flows, *Annu. Rev. Fluid Mech.*, *19*(1), 53–74, doi:10.1146/annurev.fl.19.010187.000413.

Bressan, A. (2011), Hyperbolic conservation laws, in *Mathematics of Complexity and Dynamical Systems*, edited by R. A. Meyers, chap. 44, pp. 729–739, Springer, New York, NY, United States, doi:10.1007/978-1-4614-1806-1_44.

Brundrett, E., and W. D. Baines (1964), The production and diffusion of vorticity in duct flow, *J. Fluid Mech.*, *19*(3), 375–394, doi:10.1017/S0022112064000799.

Callander, R. A. (1969), Instability and river channels, *J. Fluid Mech.*, *36*(3), 465–480, doi:10.1017/S0022112069001765.

Cao, Z., and P. A. Carling (2002), Mathematical modelling of alluvial rivers: Reality and myth. Part 1: General review, *Proceedings of the Institution of Civil Engineers Water & Maritime Engineering*, *154*(3), 207–219.

Castro, M. J., E. D. Fernández-Nieto, A. M. Ferreiro, J. A. García-Rodríguez, and C. Parés (2009), High order extensions of Roe schemes for two-dimensional nonconservative hyperbolic systems, *J. Sci. Comput.*, *39*(1), 67–114, doi:10.1007/s10915-008-9250-4.

Chavarrías, V., G. Stecca, and A. Blom (2018), Ill-posedness in modelling mixed-sediment river morphodynamics, *Adv. Water Resour.*, *114*, 219–235, doi:10.1016/j.advwatres.2018.02.011.

Colombini, M. (1993), Turbulence-driven secondary flows and formation of sand ridges, *J. Fluid Mech.*, *254*, 701–719, doi:10.1017/S0022112093002319.

Colombini, M., and A. Stocchino (2005), Coupling or decoupling bed and flow dynamics: Fast and slow sediment waves at high froude numbers, *Phys. Fluids*, *17*(3), 036602, doi:10.1063/1.1848731.

Colombini, M., and A. Stocchino (2011), Ripple and dune formation in rivers, *J. Fluid Mech.*, *673*, 121–131, doi:10.1017/S0022112011000048.

Colombini, M., and A. Stocchino (2012), Three-dimensional river bed forms, *J. Fluid Mech.*, *695*, 63–80, doi:10.1017/jfm.2011.556.

Colombini, M., G. Seminara, and M. Tubino (1987), Finite-amplitude alternate bars, *J. Fluid Mech.*, *181*, 213–232, doi:10.1017/S0022112087002064.

Cordier, S., M. Le, and T. M. de Luna (2011), Bedload transport in shallow water models: Why splitting (may) fail, how hyperbolicity (can) help, *Adv. Water Resour.*, *34*(8), 980–989, doi:10.1016/j.advwatres.2011.05.002.

Courant, R., and D. Hilbert (1989), *Methods of Mathematical Physics, Volume 2: Differential Equations*, 852 pp., John Wiley & Sons, New York, NY, United States.

Dafermos, C. M. (2010), *Hyperbolic Conservation Laws in Continuum Physics*, no. 325 in Grundlehren der mathematischen Wissenschaften, 3 ed., 708 pp., Springer Berlin, Heidelberg, Germany.

Dafermos, C. M. (2016), Introduction to the theory of hyperbolic conservation laws, in *Handbook of Numerical Methods for Hyperbolic Problems*, *Handbook of Numerical Analysis*, vol. 17, edited by R. Abgrall and C.-W. Shu, chap. 1, pp. 1–18, Elsevier, Amsterdam, the Netherlands, doi:10.1016/bs.hna.2016.08.003.

Deigaard, R., and J. Fredsøe (1978), Longitudinal grain sorting by current in alluvial streams, *Nord. Hydrol.*, *9*(1), 7–16, doi:10.2166/nh.1978.002.

Devaney, R. L. (1989), *An Introduction to Chaotic Dynamical Systems*, 336 pp., Addison-Wesley, Boston, MA, United States.

Dietrich, W. E., and J. D. Smith (1984), Bed load transport in a river meander, *Water Resour. Res.*, *20*(10), 1355–1380, doi:10.1029/WR020i010p01355.

Einstein, H. A. (1950), The bed-load function for sediment transportation in open channel flows, *Tech. Bull. 1026*, US Department of Agriculture, Soil Conservation Service, Washington, DC, United States, 70 pp.

Einstein, H. A., and H. Li (1958), Secondary currents in straight channels, *Eos, Transactions American Geophysical Union*, *39*(6), 1085–1088, doi:10.1029/TR039i006p01085.

Elder, J. W. (1959), The dispersion of marked fluid in turbulent shear flow, *J. Fluid Mech.*, *5*(4), 544–560, doi:10.1017/S0022112059000374.

Engelund, F. (1974), Flow and bed topography in channel bends, *J. Hydraulics Div.*, *100*(11), 1631–1648.

Engelund, F. (1975), Instability of flow in a curved alluvial channel, *J. Fluid Mech.*, *72*(1), 145–160, doi:10.1017/S002211207500300X.

Engelund, F., and E. Hansen (1967), Monograph on sediment transport in alluvial streams, *Tech. Rep.*, Hydraulics Laboratory, Technical University of Denmark, Copenhagen, Denmark, 63 pp.

Engelund, F., and O. Skovgaard (1973), On the origin of meandering and braiding in alluvial streams, *J. Fluid Mech.*, *57*(2), 289–302, doi:10.1017/S0022112073001163.

Erdogan, M. E., and P. C. Chatwin (1967), The effects of curvature and buoyancy on the laminar dispersion of solute in a horizontal tube, *J. Fluid Mech.*, *29*(3), 465–484, doi:10.1017/S0022112067000977.

Exner, F. M. (1920), Zur Physik der Dünen, *Akad. Wiss. Wien Math. Naturwiss*, *129(2a)*, 929–952, (in German).

Falconer, R. A. (1980), Modelling of planform influence on circulation in harbours, in *Proc. 17th Int. Conference on Coastal Eng., 23-28 March, Sydney, Australia*, pp. 2726–2744, doi:10.1061/9780872622647.164.

Fischer, H. B. (1967), The mechanics of dispersion in natural streams, *J. Hydraulics Div.*, *96*(6), 187–216.

Fischer, H. B. (1969), The effect of bends on dispersion in streams, *Water Resour. Res.*, *5*(2), 496–506, doi:10.1029/WR005i002p00496.

Fischer, H. B. (1973), Longitudinal dispersion and turbulent mixing in open-channel flow, *Annu. Rev. Fluid Mech.*, *5*(1), 59–78, doi:10.1146/annurev.fl.05.010173.000423.

Flokstra, C. (1977), The closure problem for depth-averaged 2-D flow, in *Proc. 18th IAHR World Congress, 15–19 August, Baden-Baden, Germany*.

Fowler, A. C. (1997), *Mathematical Models in the Applied Sciences*, Cambridge Texts in Applied Mathematics, 424 pp., Cambridge University Press, Cambridge, United Kingdom.

Francalanci, S., and L. Solari (2007), Gravitational effects on bed load transport at low Shields stress: Experimental observations, *Water Resour. Res.*, *43*(3), W03424, doi:10.1029/2005WR004715.

Francalanci, S., and L. Solari (2008), Bed-load transport equation on arbitrarily sloping beds, *J. Hydraul. Eng.*, *134*(1), 110–115, doi:10.1061/(ASCE)0733-9429(2008)134:1(110).

Fredsøe, J. (1978), Meandering and braiding of rivers, *J. Fluid Mech.*, *84*(4), 609–624, doi:10.1017/S0022112078000373.

Garegnani, G., G. Rosatti, and L. Bonaventura (2011), Free surface flows over mobile bed: Mathematical analysis and numerical modeling of coupled and decoupled approaches, *Commun. Appl. Ind. Math.*, *2*(1), doi:10.1685/journal.caim.371.

Garegnani, G., G. Rosatti, and L. Bonaventura (2013), On the range of validity of the Exner-based models for mobile-bed river flow simulations, *J. Hydraul. Res.*, *51*(4), 380–391, doi:10.1080/00221686.2013.791647.

Gavrilakis, S. (1992), Numerical simulation of low-Reynolds-number turbulent flow through a straight square duct, *J. Fluid Mech.*, *244*, 101–129, doi:10.1017/S0022112092002982.

Gessner, F. B., and J. B. Jones (1965), On some aspects of fully-developed turbulent flow in rectangular channels, *J. Fluid Mech.*, *23*(4), 689–713, doi:10.1017/S0022112065001635.

Giri, S., and Y. Shimizu (2006), Numerical computation of sand dune migration with free surface flow, *Water Resour. Res.*, *42*(10), W10422, doi:10.1029/2005WR004588.

Hadamard, J. S. (1923), *Lectures on Cauchy's problem in linear partial differential equations*, 316 pp., Yale University Press, New Haven, CT, United States.

Hirano, M. (1971), River bed degradation with armoring, *Proc. Jpn. Soc. Civ. Eng.*, *195*, 55–65, doi:10.2208/jscej1969.1971.195_55.

Hoey, T. B., and R. I. Ferguson (1994), Numerical simulation of downstream fining by selective transport in gravel bed rivers: Model development and illustration, *Water Resour. Res.*, *30*(7), 2251–2260, doi:10.1029/94WR00556.

Holley, E. R. (1971), Transverse mixing in rivers, *Tech. Rep. S132*, Delft Hydraulics Laboratory, Delft, the Netherlands, 96 pp.

Ikeda, S., and T. Nishimura (1985), Bed topography in bends of sand-silt rivers, *J. Hydraul. Eng.*, *111*(11), 1397–1410, doi:10.1061/(ASCE)0733-9429(1985)111:11(1397).

Ikeda, S., and T. Nishimura (1986), Flow and bed profile in meandering sand-silt rivers, *J. Hydraul. Eng.*, *112*(7), 562–579, doi:10.1061/(ASCE)0733-9429(1986)112:7(562).

Ikeda, S., G. Parker, and K. Sawai (1981), Bend theory of river meanders. Part 1. Linear development, *J. Fluid Mech.*, *112*, 363–377, doi:10.1017/S0022112081000451.

Jagers, B. (2003), Modelling planform changes of braided rivers, Ph.D. thesis, University of Twente, Enschede, the Netherlands.

Jain, S. C. (1992), Note on lag in bedload discharge, *J. Hydraul. Eng.*, *118*(6), 904–917, doi:10.1061/(ASCE)0733-9429(1992)118:6(904).

Javernick, L., D. M. Hicks, R. Measures, B. Caruso, and J. Brasington (2016), Numerical modelling of braided rivers with structure-from-motion-derived terrain models, *River Res. Appl.*, *32*(5), 1071–1081, doi:10.1002/rra.2918.

Javernick, L., M. Redolfi, and W. Bertoldi (2018), Evaluation of a numerical model's ability to predict bed load transport observed in braided river experiments, *Adv. Water Resour.*, *115*, 207–218, doi:10.1016/j.advwatres.2018.03.012.

Jeffreys, H. (1925), The flow of water in an inclined channel of rectangular section, *The London, Edinburgh, and Dublin Philosophical Magazine and Journal of Science*, *49*(293), 793–807, doi:10.1080/14786442508634662.

Johannesson, H., and G. Parker (1989), Secondary flow in mildly sinuous channel, *J. Hydraul. Eng.*, *115*(3), 289–308, doi:10.1061/(ASCE)0733-9429(1989)115:3(289).

Jop, P., Y. Forterre, and O. Pouliquen (2005), Crucial role of sidewalls in granular surface flows: Consequences for the rheology, *J. Fluid Mech.*, *541*, 167–192, doi:10.1017/S0022112005005987.

Jop, P., Y. Forterre, and O. Pouliquen (2006), A constitutive law for dense granular flows, *Nature*, *441*, 727–730, doi:10.1038/nature04801.

Joseph, D., and J. Saut (1990), Short-wave instabilities and ill-posed initial-value problems, *Theor. Comput. Fluid Mech.*, *1*(4), 191–227, doi:10.1007/BF00418002.

1149   Kabanikhin, S. I. (2008), Definitions and examples of inverse and ill-posed problems, *J. Inv. Ill-*
1150   *Posed Problems*, *16*, 317–357, doi:10.1515/JIIP.2008.019.

1151   Kalkwijk, J. P. T., and R. Booij (1986), Adaptation of secondary flow in nearly-horizontal flow, *J.*
1152   *Hydraul. Res.*, *24*(1), 19–37, doi:10.1080/00221688609499330.

1153   Kalkwijk, J. P. T., and H. J. de Vriend (1980), Computation of the flow in shallow river bends, *J.*
1154   *Hydraul. Res.*, *18*(4), 327–342, doi:10.1080/00221688009499539.

1155   Kitanidis, P. K., and J. F. Kennedy (1984), Secondary current and river-meander formation, *J.*
1156   *Fluid Mech.*, *144*, 217–229, doi:10.1017/S0022112084001580.

1157   Knowles, J. K., and E. Sternberg (1975), On the ellipticity of the equations of nonlinear elastostatics
1158   for a special material, *J. Elast.*, *5*(3), 341–361, doi:10.1007/BF00126996.

1159   Knowles, J. K., and E. Sternberg (1976), On the failure of ellipticity of the equations for finite
1160   elastostatic plane strain, *Arch. Ration. Mech. Anal.*, *63*(4), 321–336, doi:10.1007/BF00279991.

1161   Koch, F. G., and C. Flokstra (1981), Bed level computations for curved alluvial channels, in *Proc.*
1162   *19th IAHR World Congress, 2–7 February, New Delhi, India*.

1163   Kyong, O. B., and W. S. Il (2016), On the methods for determining the transverse dispersion
1164   coefficient in river mixing, *Adv. Water Resour.*, *90*, 1–9, doi:10.1016/j.advwatres.2016.01.009.

1165   Lanzoni, S., and M. Tubino (1999), Grain sorting and bar instability, *J. Fluid Mech.*, *393*, 149–174,
1166   doi:10.1017/S0022112099005583.

1167   Lax, P. D. (1980), On the notion of hyperbolicity, *Commun. Pure Appl. Math.*, *33*, 395–397.

1168   Legleiter, C. J., and P. C. Kyriakidis (2006), Forward and inverse transformations between Carte-
1169   sian and channel-fitted coordinate systems for meandering rivers, *Math. Geol.*, *38*(8), 927–958,
1170   doi:10.1007/s11004-006-9056-6.

1171   Lesser, G., J. Roelvink, J. van Kester, and G. Stelling (2004), Development and validation of
1172   a three-dimensional morphological model, *Coastal Eng.*, *51*, 883–915, doi:10.1016/j.coastaleng.
1173   2004.07.014.

1174   LeVeque, R. J. (2004), *Finite Volume Methods for Hyperbolic Problems*, no. 31 in Cambridge
1175   Texts in Applied Mathematics, Cambridge University Press, Cambridge, United Kingdom, doi:
1176   10.1017/CBO9780511791253.

1177   Lien, H. C., T. Y. Hsieh, J. C. Yang, and K. C. Yeh (1999), Bend-flow simulation using 2D depth-
1178   averaged model, *J. Hydraul. Eng.*, *125*(10), 1097–1108, doi:10.1061/(ASCE)0733-9429(1999)125:
1179   10(1097).

Lorenz, E. N. (1963), Deterministic nonperiodic flow, *J. Atmos. Sci.*, *20*(2), 130–141, doi:10.1175/ 1520-0469(1963)020⟨0130:DNF⟩2.0.CO;2.

Lyn, D. A., and M. Altinakar (2002), St. Venant-Exner equations for near-critical and transcritical flows, *J. Hydraul. Eng.*, *128*(6), 579–587, doi:10.1061/(ASCE)0733-9429(2002)128:6(579).

Meyer-Peter, E., and R. Müller (1948), Formulas for bed-load transport, in *Proc. 2nd IAHR World Congress, 6–9 June, Stockholm, Sweden*, pp. 39–64.

Mosselman, E. (2005), Basic equations for sediment transport in CFD for fluvial morphodynamics, in *Computational Fluid Dynamics: Applications in Environmental Hydraulics*, edited by P. D. Bates, S. N. Lane, and R. I. Ferguson, chap. 4, pp. 71–89, John Wiley & Sons, Chichester, United Kingdom.

Mosselman, E., K. Sloff, and S. van Vuren (2008), Different sediment mixtures at constant flow conditions can produce the same celerity of bed disturbances, in *River Flow 2008, Proc. Int. Conference on Fluvial Hydr., 3-5 September, Cesme, Izmir, Turkey*, vol. 2, edited by M. Altinakar, M. A. Kokpinar, İsmail Aydin, Şevket Cokgor, and S. Kirgoz, pp. 1373–1377, Kubaba Congress Department and Travel Services, Ankara, Turkey.

Murray, A. B. (2007), Reducing model complexity for explanation and prediction, *Geomorphology*, *90*(3-4), 178–191, doi:10.1016/j.geomorph.2006.10.020.

Murray, A. B., and C. Paola (1994), A cellular model of braided rivers, *Nature*, *371*(54), 54–57, doi:10.1038/371054a0.

Murray, A. B., and C. Paola (1997), Properties of a cellular braided-stream model, *Earth Surf. Process. Landf.*, *22*(11), 1001–1025, doi:10.1002/(SICI)1096-9837(199711)22:11⟨1001::AID-ESP798⟩ 3.0.CO;2-O.

Nezu, I., and H. Nakagawa (1984), Cellular secondary currents in straight conduit, *J. Hydraul. Eng.*, *110*(2), 173–193, doi:10.1061/(ASCE)0733-9429(1984)110:2(173).

Nikuradse, J. (1930), Untersuchungen über turbulente strömungen in nicht kreisförmigen rohren, *Ingenieur-Archiv*, *1*(3), 306–332, doi:10.1007/BF02079937, (in German).

Olesen, K. W. (1982), Influence of secondary flow on meandering rivers, *Tech. Rep. 1-82*, Laboratory of Fluid Mechanics, Faculty of Civil Engineering and Geosciences, Delft University of Technology, Delft, the Netherlands, 67 pp.

Ottevanger, W., K. Blanckaert, W. S. J. Uijttewaal, and H. J. de Vriend (2013), Meander dynamics: A reduced-order nonlinear model without curvature restrictions for flow and bed morphology, *J. Geophys. Res., Earth Surface*, *118*(2), 1118–1131, doi:10.1002/jgrf.20080.

Paola, C. (2000), Quantitative models of sedimentary basin filling, *Sedimentology*, *47*, 121–178, doi:10.1046/j.1365-3091.2000.00006.x.

Paola, C., and M. Leeder (2011), Environmental dynamics: Simplicity versus complexity, *Nature*, *469*, 38–39, doi:10.1038/469038a.

Paola, C., P. L. Heller, and C. L. Angevine (1992), The large-scale dynamics of grain-size variation in alluvial basins, 1: Theory, *Basin Res.*, *4*(2), 73–90, doi:10.1111/j.1365-2117.1992.tb00145.x.

Parker, G. (1976), On the cause and characteristic scales of meandering and braiding in rivers, *J. Fluid Mech.*, *76*(3), 457–480, doi:10.1017/S0022112076000748.

Parker, G. (1978), Self-formed straight rivers with equilibrium banks and mobile bed. Part 1. The sand-silt river, *J. Fluid Mech.*, *89*(1), 109–125, doi:10.1017/S0022112078002499.

Parker, G. (1991), Selective sorting and abrasion of river gravel. I: Theory, *J. Hydraul. Eng.*, *117*(2), 131–147, doi:10.1061/(ASCE)0733-9429(1991)117:2(131).

Parker, G., and E. D. Andrews (1985), Sorting of bed load sediment by flow in meander bends, *Water Resour. Res.*, *21*(9), 1361–1373, doi:10.1029/WR021i009p01361.

Parker, G., and A. J. Sutherland (1990), Fluvial armor, *J. Hydraul. Res.*, *28*(5), 529–544, doi:10.1080/00221689009499044.

Parker, G., C. Paola, and S. Leclair (2000), Probabilistic Exner sediment continuity equation for mixtures with no active layer, *J. Hydraul. Eng.*, *126*(11), 818–826, doi:10.1061/(ASCE)0733-9429(2000)126:11(818).

Parker, G., G. Seminara, and L. Solari (2003), Bed load at low Shields stress on arbitrarily sloping beds: Alternative entrainment formulation, *Water Resour. Res.*, *39*(7), 1183, doi:10.1029/2001WR001253.

Phillips, B. C., and A. J. Sutherland (1989), Spatial lag effects in bed load sediment transport, *J. Hydraul. Res.*, *27*(1), 115–133, doi:10.1080/00221688909499247.

van Prooijen, B. C., and W. S. J. Uijttewaal (2002), A linear approach for the evolution of coherent structures in shallow mixing layers, *Phys. Fluids*, *14*(12), 4105–4114, doi:10.1063/1.1514660.

Qian, H., Z. Cao, H. Liu, and G. Pender (2016), Numerical modelling of alternate bar formation, development and sediment sorting in straight channels, *Earth Surf. Process. Landf.*, *42*(7), 555–574, doi:10.1002/esp.3988.

Ribberink, J. S. (1987), Mathematical modelling of one-dimensional morphological changes in rivers with non-uniform sediment, Ph.D. thesis, Delft University of Technology, Delft, the Netherlands.

Rodrigues, L., and K. Zumbrun (2016), Periodic-coefficient damping estimates, and stability of large-amplitude roll waves in inclined thin film flow, *SIAM J. Math. Anal.*, *48*(1), 268–280, doi:10.1137/15M1016242.

Rozovskii, I. L. (1957), *Flow of water in bends in open channels*, 233 pp., Academy of Sciences of the Ukrainian SSR, (in English translated by Y. Prushansky in 1961).

Saint-Venant, A. J. C. B. (1871), Théorie du mouvement non permanent des eaux, avec application aux crues des rivières et à l'introduction des marées dans leur lit, *Comptes Rendus des séances de l'Académie des Sciences*, *73*, 237–240, (in French).

Schielen, R., A. Doelman, and H. E. de Swart (1993), On the nonlinear dynamics of free bars in straight channels, *J. Fluid Mech.*, *252*, 325–356, doi:10.1017/S0022112093003787.

Seminara, G. (2006), Meanders, *J. Fluid Mech.*, *554*, 271–297, doi:10.1017/S0022112006008925.

Seminara, G., and M. Tubino (1989), Alternate bars and meandering, in *River Meandering*, edited by S. Ikeda and G. Parker, chap. 10, pp. 267–320, AGU, Washington, DC, United States, doi:10.1029/WM012p0267.

Seminara, G., L. Solari, and G. Parker (2002), Bed load at low Shields stress on arbitrarily sloping beds: Failure of the Bagnold hypothesis, *Water Resour. Res.*, *38*(11), 1249, doi:10.1029/2001WR000681.

Shields, A. (1936), Anwendung der Ähnlichkeitsmechanik und Turbulenzforschung auf die Geschiebebewegung, Ph.D. thesis, Versuchsanstalt für Wasserbau und Schiffbau, 26, Berlin, Germany, (in German).

Shimizu, Y., S. Giri, S. Yamaguchi, and J. Nelson (2009), Numerical simulation of dune-flat bed transition and stage-discharge relationship with hysteresis effect, *Water Resour. Res.*, *45*(4), W04429, doi:10.1029/2008WR006830.

Sieben, J. (1997), Modelling of hydraulics and morphology in mountain rivers, Ph.D. thesis, Delft University of Technology, Delft, the Netherlands.

Simons, D. B., and M. L. Albertson (1963), Uniform water conveyance channels in alluvial materials, *Transaction ASCE*, *128*, 65–105.

Siviglia, A., G. Stecca, and A. Blom (2017), Modeling of mixed-sediment morphodynamics in gravel bed rivers using the active layer approach: Insights from mathematical and numerical analysis, in *Gravel-Bed Rivers: Process and Disasters*, edited by D. Tsutsumi and J. Laronne, chap. 26, pp. 703–728, Wiley-Blackwell, Hoboken, NJ, United States, doi:10.1002/9781118971437.ch26.

Stecca, G., A. Siviglia, and A. Blom (2014), Mathematical analysis of the Saint-Venant-Hirano model for mixed-sediment morphodynamics, *Water Resour. Res.*, *50*, 7563–7589, doi:10.1002/2014WR015251.

Stecca, G., A. Siviglia, and A. Blom (2016), An accurate numerical solution to the Saint-Venant-Hirano model for mixed-sediment morphodynamics in rivers, *Adv. Water Resour.*, *93, Part A*, 39–61, doi:10.1016/j.advwatres.2015.05.022.

Strikwerda, J. (2004), *Finite Difference Schemes and Partial Differential Equations*, 2 ed., 427 pp., Society for Industrial and Applied Mathematics, Philadelphia, PA, United States, doi:10.1137/1.9780898717938.

Talmon, A., N. Struiksma, and M. V. Mierlo (1995), Laboratory measurements of the direction of sediment transport on transverse alluvial-bed slopes, *J. Hydraul. Res.*, *33*(4), doi:10.1080/00221689509498657.

Talstra, H. (2011), Large-scale turbulence structures in shallow separating flows, Ph.D. thesis, Delft University of Technology, Delft, the Netherlands.

Toro, E. F. (2009), *Riemann Solvers and Numerical Methods for Fluid Dynamics*, 3 ed., 724 pp., Springer-Verlag Berlin, Heidelberg, Germany, doi:10.1007/b79761.

Toro-Escobar, C. M., C. Paola, and G. Parker (1996), Transfer function for the deposition of poorly sorted gravel in response to streambed aggradation, *J. Hydraul. Res.*, *34*(1), 35–53, doi:10.1080/00221689609498763.

Veprek, R. G., S. Steiger, and B. Witzigmann (2007), Ellipticity and the spurious solution problem of k-p envelope equations, *Phys. Rev. B*, *76*, 165320, doi:10.1103/PhysRevB.76.165320.

Vreugdenhil, C. B. (1994), *Numerical Methods for Shallow-Water Flow*, 262 pp., Springer, Dordrecht, the Netherlands, doi:10.1007/978-94-015-8354-1.

de Vriend, H. J. (1977), A mathematical model of steady flow in curved shallow channels, *J. Hydraul. Res.*, *15*(1), 37–54, doi:10.1080/00221687709499748.

de Vriend, H. J. (1981), Steady flow in shallow channel bends, Ph.D. thesis, Delft University of Technology, Delft, the Netherlands.

de Vries, M. (1965), Considerations about non-steady bed load transport in open channels, *Tech. Rep. 36*, Delft Hydraulics Laboratory, Delft, the Netherlands, 10 pp.

de Vries, M. (1973), River-bed variations - aggradation and degradation, *Tech. Rep. 107*, Delft Hydraulics Laboratory, Delft, the Netherlands, 21 pp.

Williams, R. D., R. Measures, D. M. Hicks, and J. Brasington (2016), Assessment of a numerical model to reproduce event-scale erosion and deposition distributions in a braided river, *Water Resour. Res.*, *52*(8), 6621–6642, doi:10.1002/2015WR018491.

Woodhouse, M. J., A. R. Thornton, C. G. Johnson, B. P. Kokelaar, and J. M. N. T. Gray (2012), Segregation-induced fingering instabilities in granular free-surface flows, *J. Fluid Mech.*, *709*, 543–580, doi:10.1017/jfm.2012.348.